AN INVESTIGATION OF THE EFFECTS OF PERIODIC WAKE DISTURBANCES ON FLAT-PLATE BOUNDARY LAYERS

by

RONALD S. K. YIP

B.A.Sc., University of British Columbia, 1982

A THESIS SUBMITTED IN PARTIAL FULFILMENT OF

THE REQUIREMENTS FOR THE DEGREE OF

MASTER OF APPLIED SCIENCE

in

THE FACULTY OF GRADUATE STUDIES

Department of Mechanical Engineering

We accept this thesis as conforming

to the required standard.

THE UNIVERSITY OF BRITISH COLUMBIA

January 1985

22

In presenting this thesis in partial fulfilment of the requirements for an advanced degree at the University of British Columbia, I agree that the Library shall make it freely available for reference and study. I further agree that permission for extensive copying of this thesis for scholarly purposes may be granted by the head of my department or by his or her representatives. It is understood that copying or publication of this thesis for financial gain shall not be allowed without my written permission.

Department of Mechanical Engineering

The University of British Columbia
1956 Main Mall
Vancouver, Canada
V6T 1Y3

Date Feb. 4, 1985

DE-6 (3/81)

Abstract

Flat plate turbulent boundary layers disturbed by periodic moving wakes have been observed in an experimental rig mounted in a low speed wind tunnel. The wakes are produced periodically by cylinders traversing in front of the leading edge of a flat plate on which the boundary layers are measured. This is to simulate the unsteady flow pattern generated by upstream blades on the downstream blade boundary layer in an axial flow turbomachine.

Both the time-averaged and ensemble-averaged data are taken from the free stream and boundary layer at different flow conditions. Free stream steady and unsteady wakes are compared and found to be similar to each other. The wake disturbance in the free stream is a function of time and distance from the cylinder. The periodic disturbance in the inner half of the boundary layer lags behind that in the free stream. This phase lag is due to the lower convection velocity near the solid surface. Similar to a steady wake, the velocity defect of an unsteady wake is higher in boundary layer than in free stream. This results in the maximum velocity defect amplitude in the inner half of the boundary layer. Phase lag and amplitude ratio profiles of the boundary layers are plotted and found to be similar to data obtained from axial flow turbomachines. Phase-averaged velocity and turbulence intensity profiles at different phase angles between two successive wakes are shown in a series of transparencies.

Table of Contents

Abstract ii

List of Figures v

Acknowledgements viii

Nomenclature ix

1. **INTRODUCTION** 1

1.1 **Introductory Remarks** 1

1.2 **Scope of the Present Investigation** 2

2. **BACKGROUND MATERIAL AND REVIEW OF PREVIOUS WORK** 5

2.1 **Background Material on Flat Plate Boundary Layers** 5

2.2 **Previous Work on Boundary Layers in an Unsteady Free-Stream** 9

2.2.1 Studies of Fluid Flow in Experimental Axial Turbomachines 10

2.2.2 Flow Studies Using Simplified Models 12

2.2.3 Numerical Programs for Calculating Unsteady Flows 14

3. **EXPERIMENTAL APPARATUS AND INSTRUMENTATION** 15

3.1 **Experimental Apparatus** 15

3.1.1 Wind Tunnel 15

3.1.2 The Rotating Cylinder Cascade and The Flat Plate 16

3.1.3 Traverse Mechanism 17

3.2 **Instrumentation** 17

3.2.1 Boundary Layer Measurement - Hot Wire Anemometry 17

3.2.1.1 Hot Wire Calibration 19

3.2.1.2 Correction for Wall Proximity Effect 19

3.2.1.3 Determination of the Vertical Distance of Hot Wire from the Flat Plate 20

3.2.2 Phase Reference - Hall Effect Switch 20

3.3 **Signal Conditioning and Data Acquisition** 21

3.4 **An Ensemble-Averaging Technique** 22

3.5 **Data Acquisition Program** 23

4. **EXPERIMENTAL RESULTS AND DISCUSSION** 25

4.1 **Time-Averaged Measurements of Steady and Unsteady Boundary Layers** 25

4.1.1 Experimental Details 25

4.1.2 Experimental Results 26

4.2 **Ensemble-Averaged Measurements of Disturbed Free Stream and Boundary Layer** 28

4.2.1 Experimental Details 28

4.2.2 Experimental Results 29

4.2.2.1 Unsteady Wake Measurements and Comparison with Steady Wake Measurements 29

4.2.2.2 Unsteady Boundary Layer Measurements 30

4.3 **Discussion** 32

5. **CONCLUSIONS AND SUGGESTIONS FOR FUTURE WORK** 35

5.1 **Conclusions** 35

5.2 **Suggestions for Further Work** 36

FIGURES 38

REFERENCES 70

APPENDICES 73

List of Figures

1.1 Two Common Constructions of Axial Flow Turbines 39

1.2 Layout of a Conventional Low Speed Cascade Tunnel 40

1.3 Schematic Diagram of Periodic Disturbance on Turbine Stator Blades40

2.1 Schematic Diagram of Flat Plate Boundary Layer Development................41

2.2 Typical Distributions in Laminar and Turbulent Boundary Layers on a Flat Plate 41

2.3 Turbulent Boundary Layer Velocity Profiles in Semi-Log Form 42

2.4 Oscillograms of Boundary Layer Velocity Records and Instantaneous Velocity Profiles on a Compressor Stator Blade, x/C=0.5........................43

2.5 Oscillograms of Boundary Layer Velocity Records and Instantaneous Velocity Profiles on a Compressor Stator Blade, x/C=0.7........................44

2.6 Pressure Loss Coefficients Across a Turbine Rotor Blade and the Same Blade in a Linear Cascade 45

2.7 Amplitude and Phase Lag Profiles for the Boundary Layers of a Turbine Rotor Blade Suction-Surface 46

2.8 Schematic Diagram of Experimental Set-Up by Pheil, Herbst and Schroder 47

2.9 Measured Mean Velocities of Wake and Boundary Layer Interacting Flow Compared to Undisturbed Flat Plate Flow..48

2.10 Decomposition of Boundary Layer-Wake Interaction for Analyzing Self-Similarity of Wake Flow 49

2.11 Comparison of Measured Mean Velocities with Results of Finite-Difference Solution 49

3.1 Schematic Diagram of the Experimental Set-Up Used in this Study ...50

3.2 Schematic Diagram of the Unsteady Flow Produced by Wakes 50
3.3 Typical Constant Temperature Hot Wire Anemometer Bridge 51
3.4 Calibration Curve of the Constant Temperature Hot Wire Anemometer 51
3.5 Still Air Wall Correction for Hot Wire Anemometer......................................52
3.6 Method of Detecting the Contact of the Hot Wire Probe and the Aluminum Flat Plate 52
3.7 An Illustration of the Ensemble-Averaged Procedure..................................53
3.8 Data Acquisition Program Flow Chart 54
4.1 Nondimensional Time-Averaged Velocity Profiles...58
4.2 Dimensional Turbulence Intensity Profiles of Undisturbed Boundary Layer 59
4.3 Nondimensional Turbulence Intensity Profiles of Undisturbed Boundary Layer 59
4.4 Boundary Layer Development...60
4.5 Clauser Plots of Time-Averaged Velocity Profiles of Disturbed Boundary Layers...61
4.6 Ensemble-Averaged Time-Velocity Record of a Traversing Wake..........62
4.7 Nondimensional Wake Velocity Profiles 63
4.8 Nondimensional Wake Turbulence Intensity Profiles......................................64
4.9 Ensemble-Averaged Time-Velocity Records...65
4.10 Ensemble-Averaged Turbulence Intensity-Time Records..............................66
4.11 Nondimensional Phase-Averaged Velocity Profiles at Different Phase Angles...67
4.12 Nondimensional Phase-Averaged Turbulence Intensity Profiles at Different Phase Angles..68
4.13 Maximum Amplitude Ratio Profiles..69

4.14 Phase Lag Profiles 69

C.1 Typical Clauser Plot 79

LIST OF PLATES

PLATE 1 The Low Speed Wind Tunnel 55

PLATE 2 The Cylinder Cascade 55

PLATE 3 The Driving motor and Speed Reduction Gears 56

PLATE 4 Bearing Supports and Traverse Mechanism 56

PLATE 5 Flat Plate and Support 57

PLATE 6 Hot Wire Probe for Boundary Layer Measurement 57

Acknowledgements

The author wishes to express his sincere gratitude to Professor R.L. Evans for his invaluable advice and guidance throughout all phases of the investigation. Thanks are due to Professor I.S. Gartshore for his helpful discussion and references. Thanks are also due to the technical staff of the mechanical engineering department for their assistance in the construction of the experimental apparatus. Financial support for this research by the Natural Sciences and Engineering Research Council of Canada is gratefully acknowledged.

Nomenclature

C	constant in the law of the wall (= 5 to 5.6)
C_ϕ	flow coefficient ($= \bar{U}_\infty / U_B$)
d	cylinder diameter
E_c	hot wire anemometer output voltage
E_o	hot wire anemometer output voltage at zero velocity
K	von Karmen constant = 0.41
Re_d	Reynolds number based on cylinder diameter
Re_x	Reynolds number based on downstream distance from the plate leading edge
Rw	hot wire resistance
t	time
$t_{1/2}$	half-width of an unsteady wake
$\bar{T}_u$	time averaged turbulence intensity
$\tilde{T}_u$	ensemble averaged turbulence intensity
U	instantaneous velocity in x direction
$\bar{U}$	time averaged velocity in x direction
$\tilde{U}$	ensemble averaged velocity in x direction
$\bar{U}_{MAX}$	maximum velocity in a time averaged steady wake
$\bar{U}_{MIN}$	minimum velocity in a time averaged steady wake
$\tilde{U}_{MAX}$	maximum velocity in an ensemble-averaged unsteady wake
$\tilde{U}_{MIN}$	minimum velocity in an ensemble averaged unsteady wake
U_{cyl}, U_B	cylinder tangential velocity
$\bar{U}_\infty$	time averaged velocity at infinity in x direction
u	turbulent velocity in x direction

u_τ	shearing velocity $(= (\tau_w/\rho)^{1/2})$
$\Delta\tilde{u}$	ensemble averaged maximum wake amplitude
V	instantaneous velocity in y direction
v	turbulent velocity in y direction
w	turbulent velocity in z direction
x	downstream distance from the plate leading edge
x_o	downstream distance from a cylinder in front of the plate
x_o/d	distance from cylinder to cylinder diameter ratio
y	vertical distance
$y_{1/2}$	half-width of a steady wake
$y/\bar{\delta}$	nondimensionalized boundary layer vertical distance from plate
ν	kinematic viscosity
ρ	fluid density
τ_w	wall shear stress
π	parameter in Coles law of the wake
δ	boundary layer thickness at $0.9\bar{U}_\infty$
δ^*	displacement thickness
$\bar{\delta}$	time averaged boundary layer thickness
θ	momentum thickness
ω	disturbance frequency (Hz)

Chapter 1

INTRODUCTION

1.1 INTRODUCTORY REMARKS

Axial flow turbomachines, both turbines and compressors, are composed of alternate rows of stator and rotor blades in the axial direction. Two common axial flow turbine constructions are as shown in Fig.1.1. In turbines, the stator blades, or nozzles, increase the fluid tangential velocity before entering the following rotor blade row. The rotor blades then convert the fluid's stagnation enthalpy to mechanical energy through the rotation of the shaft. Axial flow compressors are constructed in a similar manner except the blades are oriented in such a way to convert shaft energy to fluid enthalpy.

The blade efficiency is usually obtained experimentally under steady conditions in a linear cascade tunnel. The blades are arranged in a cascade near the outlet of the tunnel as in Fig.1.2. A pitot-static probe in front of the cascade measures the uniform flow velocity in the tunnel upstream of the cascade. Another pitot-static probe is traversed downstream of the cascade to measure the wake profiles of one or more blades. The average values of the total pressure loss and the fluid outlet angle at each incidence angle within the working range can be calculated from the measurements.(Stuart 1952)

In a real turbomachines, the flow condition is much more complex than in a cascade tunnel. Since 3-dimensional and unsteady effects are not accounted for in cascade testing, empirical correction factors must be applied to cascade results before they are used for design purposes.

In order to improve the accuracy of turbomachine performance prediction, a better understanding of the effects is required.

One of the main differences between a real turbomachine and a cascade tunnel is the unsteady flow pattern. This unsteadiness is due to the impingement of the wake being shed from the upsteam blades onto the downstream blade surfaces. Because the upstream blades pass in front of each downstream blade at a constant frequency, the boundary layer on that blade is periodically disturbed as illustrated in Fig.1.3. In the literature, the effects of unsteady free stream flows on boundary layer development has been a popular research topic. Little work has been reported on the effect of convected periodic wake disturbances on boundary layer development, however.

The objective of this research is to observe experimentally the periodic wake-turbulent boundary layer interaction in order to better understand the basic flow mechanism. A simplified experimental model is designed and constructed to isolate the effects of the unsteadiness on the boundary layer from other flow complications. The results can hopefully make an initial contribution towards the ultimate goal of providing a more accurate procedure for blade efficiency evaluation.

1.2 SCOPE OF THE PRESENT INVESTIGATION

In this thesis, the effects of periodic wake disturbance on turbulent boundary layer development is studied. The turbulent boundary layer is developed by tripping the boundary layer near the leading edge of a zero pressure gradient horizontal flat plate surface. A horizontal flat plate is used to eliminate the effect of pressure gradient. A periodic disturbance is generated by passing horizontal circular bars parallel to the plate width in front of the leading edge at a constant frequency. Measurements of the boundary layer are made near the normal operating flow coefficient, C_{ϕ}, which is approximately equal to 0.5. Through the use of this simplified experimental model, the periodic wake-turbulent boundary layer interaction can be studied without the added complication of 3-dimensional and pressure-gradient effects.

Background material and a summary of previous work are given in Chapter 2. The first part includes background material on boundary layer development and calculation of steady boundary layer profiles on a zero pressure gradient flat plate. The second part reviews previous work in the related field. This includes the comparisons of cascade tunnel measurements with the measurements from operating axial flow turbomachines, and boundary layer growth in periodic unsteady free streams. Also, the effect of the wake from a stationary bar on flat-plate boundary layer development is reviewed. Computational methods for predicting unsteady laminar and turbulent boundary layers are also briefly discussed.

The experimental apparatus and instrumentation are described in Chapter 3. The mechanical equipment includes a low speed wind tunnel, a rotating cage for periodic disturbance generation, a flat plate for generating the boundary layer, and a traverse mechanism for moving the hot wire probe across the boundary layer. The electronic equipment includes a hot wire anemometer for flow measurement, a Hall Effect switch for phase reference, a signal conditioner and the NEFF system for data acquisition.

In Chapter 4, the experimental conditions and results are presented. The results include time averaged velocity measurements of disturbed and undisturbed boundary layers, and also ensemble-averaged time-velocity measurements of the disturbed free streams and boundary layers. The ensemble-averaged phase velocity profiles, the ensemble-averaged phase turbulence intensity profiles, the amplitude ratio and phase lag profiles are obtained from the time-velocity measurements.

Chapter 5 summarises the experimental results and suggests further work required for this study.

Chapter 2

BACKGROUND MATERIAL AND REVIEW OF PREVIOUS WORK

In order to understand and discuss the observation on steady and unsteady turbulent boundary layers, some background material and published results are presented in this chapter.

2.1 BACKGROUND MATERIAL ON FLAT PLATE BOUNDARY LAYERS

In a flow field far away from any solid boundary, the flow condition can be modelled by using potential flow theory in which viscous effects are insignificant. However, in a thin layer close to the solid boundary, fluid friction slows down the flow. This thin layer in which the velocity is ultimately reduced to zero at the wall is called the boundary layer, outside of which the real fluid behaves very much like the ideal fluid.

At the early stage of flat plate boundary layer development, i.e. at low Reynolds numbers ($Re_x = U_\infty x/\nu$), there is no mixing within the boundary layer; the fluid moves along parallel streamlines. This parallel streamline boundary layer is called a laminar boundary layer. At high Re_x, i.e. further downstream, the fluid in the boundary layer have highly irregular motions which cause mixing within the boundary layer. At moderate Re_x, spots of fluid with local irregular motions appear in the layer which is the transition region from laminar to turbulent boundary layer. The boundary layer thickness increases suddenly when the boundary layer changes from laminar to turbulent. The process of boundary layer growth is as shown in Fig.2.1.

There are many analytical and numerical solutions for steady laminar boundary layer development for different pressure gradients. The material to be discussed in this section is only on flat plate boundary layers since it is the main concern in this thesis.

For $Re_x < 10^5$, the steady laminar boundary layer can be obtained by solving the Blasius equation.

$$ff''+2f'''=0 \tag{2.1}$$

where $f(\eta)=f(y(\frac{U_\infty}{\nu x})^{1/2})$, with boundary conditions,

$$\eta=0: f=0, f'=0; \text{ and } \eta=\infty: f'=1$$

This equation has been solved numerically, and the velocity distribution of the boundary layer is as plotted in Fig.2.2.

For $Re_x > 2x10^6$, it is difficult to prevent transition from occurring even though the surface of the flat plate is smooth and the flow condition in the main stream is laminar. Unlike in the laminar boundary layer, the velocity in turbulent layer is randomly fluctuating. For a two-dimensional layer, the instantaneous velocity can be represented by equation 2.2 as in Schlichting (1968).

$$\begin{aligned} U_i &= U + u \\ V_i &= V + v \\ W_i &= w \end{aligned} \tag{2.2}$$

where U_i, V_i and W_i are the instantaneous velocities in the x, y and z directions. U and V are mean velocities and u, v and w are the fluctuating components in the x, y and z directions.

Empirical formulations for the mean velocity profiles of turbulent boundary layers on zero pressure gradient surfaces have been developed from experimental results. By substituting equations 2.2 into the Navier-Stokes equations and takng time averages an extra term known as Reynolds stress is obtained from the equations of motion. Assuming that near the wall, derivatives with respect to y are much greater than those with respect to x, the shear stress term from the equation of motion can be expressed as:

$$\frac{\tau}{\rho} = -\overline{uv} + \nu\left(\frac{\partial U}{\partial y}\right) \qquad 2.3$$

On the R.H.S. of equation 2.3, the first term is the Reynolds stress and the second term is the laminar shear stress. Moving away from the wall within the boundary layer, the turbulent Reynolds stress increases but the laminar stress decreases.

By assuming the mean velocity is a function of τ_w/ρ, ν and the wall distance, y, dimensional analysis gives the "law of the wall" which is a universal turbulent boundary layer profile within the constant stress region.

$$\frac{U}{u_\tau} = f_n\left(\frac{yu_\tau}{\nu}\right) \qquad 2.4$$

where $u_\tau = (\tau_w/\rho)^{1/2}$ (shearing velocity)

In this constant stress region right next to the wall, there is a small region known as the viscous sublayer. Experimental observation showed that:

$$\frac{U}{u_\tau} = \frac{yu_\tau}{\nu} \qquad 2.5$$

Further out from the viscous sublayer but still inside this constant stress region is the logarithmic region, the velocity profile can be formulated by using,

$$\frac{U}{u_\tau} = \frac{1}{K} \ln\left(\frac{yu_\tau}{\nu}\right) + C \qquad 2.6$$

where $K = 0.41$ (Von Karman's constant)

$C = 5.0$ to 5.6

Further away in the boundary layer from the logarithmic region, Coles has proposed a universal "law of the wake" to describe the outer layer's mean velocity profile. In this region, the boundary layer is assumed to behave like a wake or free shear layer. The complete mean profile of a fully developed turbulent boundary layer can then be described by using the Coles profile.

$$\frac{U}{u_\tau} = \frac{1}{K} \ln\left(\frac{yu_\tau}{\nu}\right) + \frac{\pi}{K} \left(w\left(\frac{y}{\delta}\right)\right) + C \qquad 2.7$$

where $w\left(\frac{y}{\delta}\right) = 2\sin^2\left(\frac{2y}{\pi\delta}\right)$

The mean velocity profiles of the three regions in a turbulent boundary layer are plotted in semi-log form in Fig.2.3.

For a flat plate turbulent boundary layer with Re_x around 10^5, the mean velocity profile can also be approximated by the Power Law form.

$$\frac{U}{U_\infty} = \left(\frac{y}{\delta}\right)^n \qquad 2.8$$

with n= 1/7, which was obtained empirically by Nikuradse (Schlichting 1979), Fig.2.2

The above representation of the boundary layer velocity profiles is only for steady freestream flows. The effect of periodic wakes on turbulent boundary layers will be discussed in a later section and the time averaged profiles of the disturbed boundary layer will be compared with the above steady velocity profiles to observe the effect of the disturbances on the mean boundary layer development.

2.2 PREVIOUS WORK ON BOUNDARY LAYERS IN AN UNSTEADY FREE-STREAM

There has been tremendous interest in trying to understand the behavior of blade boundary layers in the highly unsteady and turbulent flow pattern in axial flow turbomachines. A review of the literature has found no numerical or analytical prediction methods for unsteady wake disturbed turbulent boundary layers. However, various authors have published papers on related topics. These papers are classified into three main groups which include; studies of fluid flow inside experimental turbomachines, studies of fluid flow in simplified experimental models, and studies using numerical computational methods for predicting the boundary layers in unsteady freestream flows.

2.2.1 STUDIES OF FLUID FLOW IN EXPERIMENTAL AXIAL TURBOMACHINES

Evans (1974) measured turbulence and unsteadiness of the flow downstream of the moving blades in a single stage 22 blade experimental compressor. By using an ensemble averaging technique, he was able to separate the random turbulence from the periodic unsteadiness. In another paper, Evans (1977) used a compressor which has a 24 blade rotor followed by a 15 blade stator to study the effects of the rotor blade wakes on the stator blade boundary layer development. The results were compared to the results of similar blades in a cascade tunnel. The boundary layer integral parameters, such as δ^*, θ, and C_f were higher in the compressor measurements than in the cascade measurements. The higher momentum loss of the compressor blade in an operating machine is thought to be caused by the wake disturbance from the rotor blades upstream. By using the ensemble averaging technique, instantaneous velocity profiles at the maximum (0°), and the minimum (180°) freestream velocities were obtained by reading the velocities of the required angle from a series of ensemble-averaged velocity records which were taken at different vertical distances from the plate, as shown in Fig.2.4. In the lower part of the boundary layer, the fluctuation were 180° out of phase with the free stream. This phase-shift phenomenon disappeared further downstream when the boundary layer was fully turbulent, as can be seen in Fig.2.5.

Hodson (1982) made boundary layer measurements on a rotor blade in a low speed, single stage, axial flow turbine. The results were compared to those of a cascade with the same blades in a steady flow. Fig. 2.6 shows that the rotor relative loss coefficient in the turbine is higher than the mass-weighted profile loss coefficient obtained from the cascade tunnel test. The integral parameters were found to be higher than the cascade results. In the boundary layer measurements, he showed that the wake induced fluctuation has a maximum amplitude within the boundary layer on the suction side of the rotor blade. Fig. 2.7 shows the amplitude ratio ($=\Delta\tilde{u}/\bar{U}_\infty$) against distance from plate surface, y. This amplitude also increases in the downstream direction. The amplitude of the wake fluctuation approaches zero near the surface because of the damping of the surface shear stress. Similar to the 180° out of phase observed by Evans (1977), he also observed a phase lag increase between the wake disturbance and the freestream towards the blade surface and from the leading edge to the trailing edge, Fig.2.7. However, unlike Evans' result, this phase lag did not disappear further downstream.

Although the negative effects of the unsteady disturbances on the aerodynamic efficiency of blades in turbomachines are obvious, the basic mechanism of the wake-boundary layer interaction is still not well understood. Researchers have tried to use simplified models to gain better understanding of this basic mechanism.

2.2.2 FLOW STUDIES USING SIMPLIFIED MODELS

Many experiments have been performed to study the effects of different unsteady freestreams on flat plate turbulent boundary layer development.

Karlsson (1958) investigated the effects of a free stream oscillation which is a function of time only on a flat plate boundary layer. The results show that the non-linear interaction between the oscillating amplitude and the boundary layer is small. The boundary layer of an instantaneous free stream velocity in an oscillating cycle does not deviate very much from that of a steady free stream of equal velocity.

Patel (1975) used an oscillating wind tunnel nozzle extension to create convected freestream oscillations of the following form,

$$U(x,t)= U_o(1 + N \sin \omega(t-x/\Omega)) \qquad 2.9$$

where U is the flow velocity as a function of downstream distance x and t. U_1 is freestream oscillation amplitude. U_o is mean velocity. $N(=U_1/U_o)$ is the ratio of the wave amplitude to mean freestream velocity. ω is the radian frequency and Ω is the travelling wave convection velocity. Flat plate turbulent boundary layers were measured. Amplitude ratio and phase lag profiles similar to those of Hodson (1982) were obtained. It was observed that the maximum amplitude ratio increases with ω but does not depend on U_1. On the contrary, the maximum phase lag does not depend on the amplitude ratio only when it is less than 0.5%. The effects of ω

and downstream distance on maximum amplitude ratio and phase lag angle can be collapsed by using the reduced frequency parameter, $\omega x/U_o$.

Pfeil, Herbst and Schröder (1982) developed an analytical model to describe the transition process from a laminar to a turbulent boundary layer under periodic wake induced fluctuations. Experiments were carried out to confirm the model. In the experiment, the rotor blades were simplified to bars of a rotating cage and the stator blade to a flat plate as in Fig 2.8. The transition mechanism of a zero pressure gradient and a favorable pressure gradient boundary layer were studied and found to agree with the model.

Marumo, Susuki and Sato (1978) as well as Tsiolakis, Krause and Müller (1983) studied the effects of the wake from a stationary bar on a fully developed turbulent flat plate boundary layer. The bar was placed at different vertical distances from the plate. A hot wire anemometer probe was traversed through the boundary layers at different downstream positions in both experiments. Marumo et al (1978) took measurements at $x/d=4.6$ to 105 and Tsiolakis et al (1983) took measurements at $x/d=20$ to 86. The results from both reports show that the nearwall region of the disturbed boundary layer recovers much faster than the outer region. Fig.2.9, which is taken from Tsiolakis (1983), shows the difference in profiles of the undisturbed layer and the disturbed layer with the stationary bar placed at two different distances from the plate. The results showed that the self-similarity of a distorted boundary layer can be modelled by assuming the boundary layer flow to be created by a velocity defect $\Delta_1\bar{U}$, Fig.2.10. The flow of the wake of the cylinder, $\Delta_2\bar{U}$, can be superimposed to the first approximation to yield the resultant velocity defect, $\Delta\bar{U}$. This model reasonably approximated the self-similar upper part of the inner layer, but it broke down in the nearwall region because of the non-linearity and large velocity defect close to the wall.

2.2.3 NUMERICAL PROGRAMS FOR CALCULATING UNSTEADY FLOWS

Evans (1974) developed a numerical computation program to calculate the development of turbulent boundary layers in different freestream turbulent intensities. The predicted results closely agree with experimental results of compressor cascade boundary layers. However, this does not give adequate prediction on boundary layer under periodic wake disturbance. A computer program was written by Cebeci and Carr (1978) to calculate laminar and turbulent boundary layers for two dimensional time-dependent free stream flows. Patel (1975) closely predicted the phase lag and amplitude ratio profiles of boundary layers in quasi steady and high frequency free stream oscillations of the form of equation 2.10. Tsiolakis, Krause and Müller (1983) solved the boundary layer equation with an implicit finite-difference method developed at the Aerodynamisches Institute of Technical University, Aachen, to obtain mean velocity profiles of distorted boundary layers, as shown in Fig.2.11. Good agreement between the computed mean velocity profiles and experimental data was obtained.

Chapter 3

EXPERIMENTAL APPARATUS AND INSTRUMENTATION

3.1 EXPERIMENTAL APPARATUS

The study of the effects of periodic disturbance on blade performance in operating turbomachines is very difficult because of the complicated flow pattern. In order to isolate this particular flow condition, a suitable experimental model must be selected. Among the experimental studies on unsteady flows, the experimental set-up used by Pfeil et al (1982), Fig.2.8, was considered to be the most compatible with the available wind tunnel in the laboratory. However, in order to avoid the flow being disturbed twice, the flat plate is installed inside the rotating cascade in this experiment, as shown in Fig.3.1. Wakes are generated periodically and carried downstream along the plate at the convection velocity when the cylinders pass in front of the leading edge of the plate at a constant frequency, Fig.3.2.

3.1.1 WIND TUNNEL

A low-speed open wind tunnel, Plate 1, in the aerodynamics laboratory of the University of British Columbia is used to generate the air flow required in this experiment. The dimensions of the test section is 45.7 cm x 45.7 cm and 190.5 cm long. Two pairs of windows are on the tunnel walls of the test section. The pair of windows at the upstream is removed for the installation of the apparatus. The tunnel's contraction ratio between the intake and the test section is high and the empty tunnel turbulence intensity is about 0.3%. The air flow velocity ranges from 0 m/sec to 20 m/sec and the mean convection velocity profile is slightly higher near the ceiling of the tunnel. However, the effect of this slight velocity variation is assumed to be negligible since the measurements are made only near the center of the cross section.

3.1.2 THE ROTATING CYLINDER CASCADE AND THE FLAT PLATE

The rotating cylinder cascade is composed of two circular end plates of 43.2 cm in diameter and aluminum cylindrical rods of 0.635 cm in diameter. The rods are arranged at a distance of 28.4 cm apart from each other, Plate 2. The cascade is driven by a variable speed direct current motor with a speed reduction sprocket and chain drive. The cascade rotational speed ranges from 0 to 1000 rpm. The cascade is connected to the driving system at one side of the tunnel, Plate 3. The other side of the cascade is supported by three external bearings. The alignment of the cascade and the sprocket is done by adjusting the distance of the bearings from the center of rotation, Plate 4. On the same side as the external bearings, there is a platform for mounting the traverse mechanism and and the flat plate inside the rotating cascade. The plate used is aluminum of 0.635 cm thick and has a chord length of 33 cm with a round leading edge. A tripping wire is glued on to the plate near the leading edge to ensure the boundary layer is turbulent. The plate is reinforced by a channel under it to eliminate the vibration induced by the rotation of the motor and the wind load. Holes are cut from the flanges of the channel to reduce its obstruction in the air flow, Plate 5.

3.1.3 TRAVERSE MECHANISM

A mechanism is used to traverse the hot wire probe for fluid velocity measurement. The vertical displacement of the probe is measured by a Mitutoyo 197-201 micrometer head with a non-rotating spindle. The micrometer has a 2 inches travel capacity with a smallest division of 0.0002 inches on the thimble. An extension is connected to the end of the spindle to hold the probe inside the tunnel. Precaution has been taken to place the probe far away from both end plates so that their effect on the boundary layer can be neglected. The horizontal movement is obtained by sliding the micrometer along a horizontal rectangular bar mounted on the platform. A clear acrylic window box is used to cover the entire assembly during the experiment. The access to the micrometer inside the box is by a stem which protrudes the top of the window box from the micrometer.

3.2 INSTRUMENTATION

3.2.1 BOUNDARY LAYER MEASUREMENT - HOT WIRE ANEMOMETRY

Low frequency response devices, such as pitot-static tubes, is not suitable for measuring high frequency periodic velocity and are not used in this experiment. However, hot wire anemometry, which is a standard technique to measure unsteady fluid flow, is used here because of its high frequency response. A constant temperature anemometer is used in this experiment. The schematic circuit is as shown in Fig.3.3. The voltage at C, E_c, increases as the air speed increases and decreases as air speed decreases. The velocity-voltage relationship is according to the following expression.

$$E_c^2 = A^2 + BU^n \qquad 3.1$$

with A, B and n are constants to be obtained from the calibration of the hot wire.

The frequency response of a hot wire system can be increased by increasing the overheat ratio which is given by the expression, $(Rw_{heated}-Rw_{ambient})/Rw_{ambient}$. However, if the system is too sensitive, i.e. the overheat ratio is too high, it tends to burn wires.

The hot wire used in this experiment is a Disa 55P15 boundary layer probe with a 5 μm diamemter and 1.25 mm long platinum plated tungsten wire, Plate 6. The bridge is Disa 56C16 general purpose bridge. The frequency response of the hot wire bridge without the wire is about 100 kHz which is assumed to be high enough for the periodic unsteady frequency, which is in the order of 200 Hz in this experiment. The spatial resolution based on the length of the wire and free stream velocity gives the cut-off frequency at about 8000 Hz. The conversion from voltage to velocity of equation 3.1 is done in a data acquisition program.

3.2.1.1 Hot Wire Calibration

The hot wire calibration is done in the empty wind tunnel before the rest of the apparatus is installed. The mean air flow velocity is measured by a pitot-static tube. The constant A in equation 3.1 is the voltage output at zero velocity. Two sets of velocities and voltages from the upper range and lower range of velocities are required to determine the constants B and n in the voltage-velocity calibration expression, equation 3.1. The calibration curve is compared with the velocity-voltage experimental data points in Fig.3.4. The ambient temperature variation in the laboratory is assumed to be too small to have any effect on the hot wire calibration.

3.2.1.2 Correction for Wall Proximity Effect

Because the heat transfer rate of the hot wire increases when it is close to a solid boundary, the hot wire signal must be corrected when it is used in boundary layer measurement. The still-air correction technique used by Hodson (1982) is used here. The hot wire output voltages in still air at various distances from the surface are measured. The calibration curve is then modified to give the following equation;

$$E_c^2-A^2-(E_o^2(y)-E_o^2(\infty))=BU^n \qquad 3.2$$

where $E_o(y)$ is the hot wire voltage output at the vertical distance, y, from the surface in still air. Since $A=E_o(\infty)$, equation 3.2 can be simplified to

$$E_c^2-E_o^2(y)=BU^n \qquad 3.3$$

$E_o(y)$ is measured and a cubic spline fitted before any boundary layer measurements. The coefficients from the cubic spline curve fitting of the data are stored in the data acquisition program for correcting the hot wire signals. The variation of the still air hot wire output, E_o, with the vertical distance, y, from the aluminum plate surface is shown in Fig.3.5. The data show that the solid surface affects the hot wire output only when the wire is less than 3 mm from the plate surface.

3.2.1.3 Determination of the Vertical Distance of Hot Wire from the Flat Plate

The distance between the hot wire and the flat plate is measured by the Mitutoyo micrometer. The zero offset value is the reading on the micrometer head when the hot wire prongs touch the plate surface. The contact of the prongs and the aluminum flat plate is detected by an ohmmeter which is connected between the prongs and the surface, as in Fig.3.6. The resistance drops from infinite to some finite value when the prongs touch the plate. The two prongs are aligned on the same plane by eye. The zero position reading is subtracted from the micrometer reading at each position to obtain the true distance from the plate.

3.2.2 PHASE REFERENCE - HALL EFFECT SWITCH

Because of the continuous rotation of the cascade, a reference point on the cascade is required to indicate the starting point of each revolution for data acquisition purpose. A UGN-30197 Hall Effect Digital switch is used in this application. This device is a 3-pin single output integrated circuit. The first pin is the input pin to which 9 V D.C. is applied. The second pin is the ground. The third pin is the output which is normally high but drops to zero when it senses a magnetic field. The voltage drop is nearly instantaneous so that the response time is assumed to be zero. The switch is mounted facing the sprocket on the cascade. A piece of magnet is glued on the sprocket. Since the cascade and the sprocket are rotating at the same angular speed, the switch voltage drops at the same instant in each revolution when the magnet passes in front of the switch. The switch output voltage is fed into the computer to be sampled by a data acquisition program to signal the start of a data acquisition cycle.

3.3 SIGNAL CONDITIONING AND DATA ACQUISITION

A high speed data acquisition system, NEFF, is used to first digitize the input signals, and then send the digitized signals to a PDP 11 computer for further processing. The input signals are from the hot wire anemometer and the Hall Effect switch through two channels. The maximum sample size is 4096 and the maximum sampling frequency is 20kHz using multi-channels. Because the NEFF's maximum range of input voltage is 1 V, a Disa 55D25 signal conditioner is used to subtract an offset voltage, 1.3 V, from the hot wire output signal and then linearly amplify the difference. The minimum and the maximum hot wire output signals are monitored by using a Tektronix 434 storage oscillocope throughout the experiment to make sure the signal is within the voltage range.

3.4 AN ENSEMBLE-AVERAGING TECHNIQUE

The NEFF system enables one continuous record of hot wire output in a period of time to be read by a data acquisition program at a time. However, these records are the sum of the random turbulence fluctuation and the periodic unsteadiness, the effect of the periodic unsteadiness on the boundary layer cannot be seen clearly unless the records are ensemble-averaged. The ensemble-averaging technique is used to suppress the non-periodic fluctuation in the data to obtain the 'clean' periodic unsteadiness in the boundary layer.

The ensemble-averaging technique requires a number of hot wire records which are taken at the same location and sampled within the same period of time in each revolution as shown in Fig.3.7.a. Since the timer-average of the random component of a fluctuating velocity approachs zero, the random velocity fluctuation can be eliminated from the periodic unsteadiness by calculating the mean velocity of a large number of records taken at the same instant of each cycle. The ensemble-averaged velocity as a function of time is then given by;

$$\tilde{U}(t)=(\sum_{i}^{N} U_i(t))/N \qquad 3.4$$

The number of records, N, is chosen so that a further increase in N will not further reduce the random fluctuation in the ensemble averaged records. Similar to the ensemble averaged velocity, a record of random turbulence intensity as a function of time at the same location can also be obtained after the ensemble-averaged velocity has been obtained.

$$\tilde{T}_u(t)=((\sum_{i}^{N}(U_i(t)-\tilde{U}(t))^2)/N)^{0.5}/\ \tilde{U}(t) \qquad 3.5$$

$U_i(t)-\tilde{U}(t)$ is the random velocity fluctuation in the flow at time, t and is designated as u in Fig.3.7.b. Because each ensemble-averaged wake disturbance is identical and periodic, each instant within one cycle can be referred to as a phase angle which varies from 0° to 360°. Ensemble-averaged velocity profiles and turbulence intensity profiles at a particular phase angle can be obtained by stacking a number of ensemble-averaged records, which are obtained from different vertical distances from a surface, and "slicing" at the required phase angle. The above signal processing is carried out in a data acquisition program as described in the following section.

3.5 DATA ACQUISITION PROGRAM

The data acquisition program is shown by the flow chart shown in Fig.3.8. A test subroutine is included to check if both channels are working properly by sampling two known signals through the two channels. The program converts digitized hot wire output back to velocity unit. In order to do the wall proximity correction, $E_o(y)$ in equation 3.4 is calculated from the cubic spline fitted curve for wall proximity effect which has been discussed in section 3.2.1.b. Because of the huge amount of data required, the time to carry out the conversion must be cut as short as possible during the experiment. Instead of repeating the above conversion for each digitized input point, the corresponding velocity is obtained from a "look-up" table which consists of the precalculated velocity values for digitized voltage between 0 and 1 V. This procedure can speed up the conversion by a factor of 10. Moreover, in order to do the ensemble-averaging procedure as discussed in section 3.4, all records have to start at the same instant during each revolution. The records are synchronized by scanning the Hall Effect switch output for the jump from the low to high state. Each hot wire record is added to the previous one, so only the ensemble-averaged velocity cord is left in the data array at the end. The ensemble-averaged turbulence intensity record is obtained by repeating the data acquisition cycle. But instead of adding to the previous hot wire record, the ensemble-averaged velocity obtained above is subtracted from the new hot wire record before adding, as shown in equation 3.5. The ensemble-averaged records are then stored in floppy diskettes.

Chapter 4

EXPERIMENTAL RESULTS AND DISCUSSION

4.1 TIME-AVERAGED MEASUREMENTS OF STEADY AND UNSTEADY BOUNDARY LAYERS

4.1.1 EXPERIMENTAL DETAILS

During the experiment, free stream velocities of U_∞ = 8.4 m/s and 11.7 m/s were used to produce boundary layers on a flat plate. The undisturbed and disturbed boundary layer profiles were measured at 100 mm and 200 mm downstream from the leading edge of the plate. The Reynolds numbers, Re_x, corresponding to the above conditions were approximately at 0.5×10^5, 0.7×10^5, 1.0×10^5 and 1.4×10^5. The unsteady boundary layer was disturbed by the cascade cylinders at a frequency of 50 Hz (i.e. tangential velocity, U_B, of the cylinder is at 14 m/s.). The flow coefficient, $C_\phi(=U_\infty/U_B)$, was at 0.57 and 0.84 respectively for the two cases of free stream velocities. The hot wire probe was traversed across the boundary layer to obtain the time-averaged velocity and turbulence intensity profiles. The time-averaged hot wire voltage output was obtained by using a Disa 56N22 Mean Value Unit with an integral time of 10 seconds. The time-averaged voltage was then converted to velocity units as described in section 3.2.1. The time-averaged turbulence intensity was obtained by feeding hot wire output voltage to a Disa 55D35 RMS voltmeter. Since the hot wire anemometer was not linearized, the voltmeter reading from the RMS meter was calibrated according to appendix A to obtain the true turbulence intensity.

4.1.2 EXPERIMENTAL RESULTS

The non-dimensional time-averaged velocity profiles of disturbed and undisturbed boundary layers are shown in Figs.4.1.a and 4.1.b. Without any disturbance, the boundary layer is not quite turbulent even with the tripping wire. This is because of the Reynolds numbers for the short plate. For the case in which the free stream is disturbed by the motion of the cascade cylinders, the turbulence level is intensified. The disturbed boundary layers are closer but not quite equal to the fully developed turbulent boundary layer which can be represented by the 1/7-th Power Law as discussed in section 2.1.

Figs.4.2 shows the turbulence intensity profiles of the undisturbed boundary layer. In Fig. 4.3, the y distance is nondimensionalized by the time-averaged boundary layer thickness. The extraordinarily high turbulence intensity near the surface requires more careful consideration because the highest turbulence intensity is usually about 0.4 within a short distance from a tripping wire and the highest reading obtained in this experiment is around 0.7. The dimensional plot shows that because of the mixing of the highly turbulent fluid particles in the inner boundary layer and the low turbulent fluid in the free stream, the turbulence intensity increases in the outer layer and decreases in the inner layer as the fluid moves downstream. The nondimensional plot shows that although the high turbulence intensity fluid diffuses into the free stream, the rate is not as fast as the growth of the boundary layer thickness. Consequently, the turbulence intensity at any point on a nondimensional profile is lower than that of a corresponding point on a profile of lower Reynolds number.

The displacement and momentum thickness, δ^* and θ, are determined according to appendix B. Fig.4.4 shows the increase of the displacement and momentum thickness of the disturbed and undisturbed boundary layers. The results at 100 mm and 200 mm are joined by straight lines to show the general trend. The integral parameters of the undisturbed case start at a smaller value when compared to the disturbed boundary layer but they grow a lot faster. A higher momentum thickness indicates a higher momentum loss in the boundary layer. An estimation of surface shear stress by using Clauser plots has been attempted. This technique is discussed in appendix C. However, as shown in Fig.4.5a and 4.5b, the linear region is not apparent in the disturbed profiles because of the low Reynolds numbers used in this experiment. Therefore, it is concluded that the boundary layer profiles are not fully turbulent and are different from "the Law of the Wall". As a result, the estimated values of the surface shear stresses are not accurate and are not shown.

4.2 ENSEMBLE-AVERAGED MEASUREMENTS OF DISTURBED FREE STREAM AND BOUNDARY LAYER

4.2.1 EXPERIMENTAL DETAILS

The flat plate was removed from the experimental rig for taking the unsteady free stream measurements. The conditions were as discussed in section 4.1.1. The x_o/d ratios (where x_o is the downstream distance from the bar and d is the cylinder diameter) were 25 and 41, corresponding to the 2 positions, 100mm and 200mm downstream of the leading edge. The Reynolds number based on the cylinder diameter, Re_d, was 3600 and 5000 respectively. The velocity signals were ensemble-averaged as the bars passed in front of a stationary hot wire probe using the technique in section 3.4. The wake from a stationary cylinder was also measured to compare with the moving wake which was created by the rotating cylinder cascade.

The experimental conditions for unsteady boundary layer measurements were also as described in section 4.1.1. The hot wire probe was traversed across the boundary layers and the signals were ensemble-averaged to give the average velocity and turbulence intensity at each instant in a cycle. 175 records were used for each ensemble-averaged record in both the free stream and boundary layer measurements. The phase-averaged velocity and turbulence intensity profiles at the required phase angle were then obtained as discussed in section 3.4

4.2.2 EXPERIMENTAL RESULTS

4.2.2.1 Unsteady Wake Measurements and Comparison with Steady Wake Measurements

Fig.4.6 shows the ensemble-averaged velocity record for the moving wakes which were caused by the cylinders passing in front of the stationary hot wire probe. The random turbulence is suppressed and the periodic velocity defects created by the motion of the cylinders are clearly shown. Since the cascade cylinders traverse in front of the hot wire probe, each velocity defect is a wake from a passing cylinder. Similar to stationary wakes, the moving wakes are symmetrical as well.

Fig.4.7 shows the nondimensional steady and traversing wake profiles. The experimental results are compared with the theoretical wake profile as described by Reichardt (Schlichting 1979). The velocity axis is nondimensionalized as shown on the graph. The width of the steady wakes are nondimensionalized by their half-widths, $y_{1/2}$, and the traversing wakes are by the half-times, $t_{1/2}$, which is the time for the wakes to move from the minimum velocity to half way between the maximum and minimum velocity. Self-similarity of the wakes is not expected because of the small x_o/d ratio. However, the nondimensional wake profiles are plotted to show that the traversing wakes do resemble the steady wakes. This shows that the cylinder's tangential velocity determines how fast the wakes traverse across the hot wire probe but has very little effect on the shape of the wake.

Fig.4.8 shows the turbulence intensity in both the nondimensional traversing and steady wakes. The turbulence intensity distributions in the traversing wakes are similar to those of steady wakes. Similar to the velocity distributions of the traversing wakes, there is an unexpected increase of turbulence before each main wake. The turbulence intensity of the traversing wakes are about 25% higher than the steady ones.

4.2.2.2 Unsteady Boundary Layer Measurements

Fig.4.9 shows the ensemble-averaged velocity records at different positions across a disturbed boundary layer. The wakes are less symmetrical than the moving wakes in the free stream. The velocity decreases sooner and more slowly than it increases. In the inner part of the boundary layer, the wakes arrive at the measuring point later than those in the outer layer due to the lower convection velocity in the inner layer. This delay is quantified in terms of degrees of phase lag relative to the free stream disturbance. A full 360° is defined as the period between two successive wakes, as shown in Fig.4.9.

Fig.4.10 shows the ensemble-averaged turbulence intensity records at the same positions at which the velocity records were obtained. The turbulence level between the wake disturbances is similar to that of steady turbulent boundary layers as shown in Figs.4.2 and 4.3. When a wake passes the measuring probe, the turbulence intensity rises quickly. As the probe is moved closer to the surface, the rms turbulence intensity between wakes increases, and finally, the wake disturbance disappears within the overall turbulence intensity. The phase lag of the wakes in the inner layer can also be seen from these turbulence intensity records.

Figs.4.11 and 4.12 show the phase-averaged velocity and turbulence profiles at every 60° phase angle in a cycle from 0° to 360° as designated in Fig.4.9. The profiles are obtained by reading off velocity values from each record at the required phase angle. The profiles are shown in a series of overlapping transparencies so that the change in profiles at each 60° phase angle can be clearly seen. At 0°, the velocity of the profile is the lowest because the cylinder has just traversed in front of the boundary layer. At 60°, the wake is outside the boundary layer and the free stream velocity profile has increased to its maximum value. However, the inner layer cannot respond as fast as the outer layer, and the inner layer velocity does not reach the maximum value until 120°. This is the consequence of the phase lag characteristics of wake disturbance in the inner layer. The phase lag phenomenon has already been observed from Fig.4.9 and 4.10. For the same reason, the outer layer velocity starts to decrease sooner than the inner layer at 180° as another wake starts to move through the boundary layer. This reduction in the outer layer profile continues to 240° phase angle, and then at 300°, the inner layer also starts to show a reduced velocity. At 360°, the velocity profile is again fully retarded in the middle of the wake, and is essentially the same as the 0° profile.

In Fig.4.12, the phase-averaged turbulence intensity profiles are shown at increments of 60° phase angles on a series of transparencies. At 0°, the turbulence level is high and evenly distributed since the wake has just moved across the boundary layer. As the wake has moved away, the intensity decays slowly. In between wakes, at 180° and 240°, the phase-averaged turbulence intensity profiles are similar to those of the undisturbed boundary layers as shown in Fig.4.2 and 4.3. The turbulence intensity increases again as the next wake is approaching at 300°. At 360°, the intensity profile is again fully increased to the profile at 0°.

Fig.4.13 is plotted to show how the maximum velocity defects of wakes change with vertical distances from the plate. The defect amplitude is the difference between the ensemble-averaged maximum and minimum velocity in a wake. The result shows, as expected, that the amplitude ratios are close to constant in the free stream and zero at the plate surface. There is a maximum amplitude ratio in the lower half of the boundary layer. Because of the decay of the wakes, the amplitude ratios decrease with x_o/d.

The phase lag phenomenon which has been observed previously in Figs.4.9 and 4.10 is plotted in Fig.4.14 to show how the phase lag changes with distances from the plate. The phase lag measured is relative to the record near the free stream. The phase lag starts to occur at about half way down the boundary layer and increases toward the surface. The phase lag profiles also appear to increase with Re_x, i.e. the phase lag is higher as the boundary layer profile is measured farther away from the leading edge.

4.3 DISCUSSION

Even in this simplified model, the flow pattern is complicated due to the periodic disturbance of the wakes generated by the moving bars. The free stream measurements show that the moving wake is similar to the steady wake. The free stream velocity at any point is, therefore, a funtion of time, t, beacuse of the periodic nature of the wake and the distance from the cylinder, x_o, because of the decay of the maximum wake amplitude with distance from the bar. Consider the observation of a wake generated by a particular bar starts at time, $t=0$, when the bar is immediately above the plate. The wake is carried downstream by the main flow. However, as the wake enters the boundary layer, the velocity slows down on the plate surface and the wake is distorted by the viscous shear stress. A short time later, Δt, the bar has moved a small distance farther away from the plate and the wake at this point is carried downstream at a higher velocity since the fluid particles are farther away from the surface. As a result, the wake disturbance in the inner layer lags behind the outer layer disturbance, as shown in Fig.4.9 and the phase lag relationship with distance from the plate is as shown in Fig.4.13. This phase lag behavior has also been observed by Hodson (1982), Fig.2.7.

Even at low Reynolds numbers, the presence of the periodic wakes make the time-averaged boundary layer profiles closer to a fully developed turbulent boundary layer because of the periodic increase of the turbulence intensity. The integral boundary layer parameters agree with the data obtained by Evans (1974) and Hodson (1982) showing the maximum loss in the wake disturbed boundary layer to be higher than in the undisturbed case. Since the wakes are velocity defects, their periodic existence in the boundary layer decreases the time-averaged velocity and thickens the boundary layer, especially at the early part of the boundary layer where the wake has high velocity defect.

At constant free stream velocity and cylinder diameter, the wake amplitude ratio is a function of x_o/d only. The amplitude ratio in the free stream at each x_o is constant while on the surface, the amplitude ratio is zero because the velocity is zero due to the no-slip condition. Within the boundary layer, the interaction between a wake from a stationary bar and the boundary layer can be described by the theoretical model as shown in Fig.2.10. As measured by Tsiolakis et al (1983), when the centerline of the steady wake is in the boundary layer, the maximum velocity defect is larger than the free stream velocity defect as can be observed in Fig.2.9. As a result, there is a maximum wake amplitude somewhere within the boundary layer. The maximum amplitude has been found to be within the inner half of the boundary layer from the experimental data reported here. Hodson (1982) has observed a similar unsteady wake and boundary layer interaction on a turbine rotor blade surface, Fig.2.7. Moreover, the overall amplitude ratio profile decreases with distance from the cylinder because of the decay of the wake. Further, because each phase-averaged boundary layer profile is a profile at a particular phase in the disturbance, one would expect the profile to look similar to Fig.2.9 which shows the existence of the wake in the boundary layer. However, due to the phase lag in the inner layer, the kind of profile obtained in the steady experiments of Tsiolakis et al does not exist.

Chapter 5

CONCLUSIONS AND SUGGESTIONS FOR FUTURE WORK

5.1 CONCLUSIONS

Some insight into the foundamental behavior of a boundary layer in a free stream which is periodically disturbed by traversing wakes have been obtained. The unsteadiness causes the time-averaged boundary layer profiles to be closer to fully turbulent even at low Reynolds numbers. The periodic existence of the wake defects in the flat plate boundary layer causes the dramatic increase of displacement and momentum thicknesses, especially in the early part of the boundary layer. The difference is less farther downstream because of the decay of the wake. The moving wakes created by the rotating cylinder cascade have been observed and found to be closely similar to the steady wakes. The disturbance at any point in the free stream is a function of time according to the shape of the wakes and distance from the cylinder which is source of the wake. The wake's effects on the boundary layer development have been shown in a series of phase-averaged velocity and turbulence intensity profiles at every 60° phase angle between two successive wakes. The shape of these profiles are determined by the relations of the phase lag and maximum wake amplitude ratio with the distance from the surface which have also been observed in this study. The phase lag and maximum wake amplitude ratio profiles are similar to those obtained in operating turbomachines by previous researchers. The phase lag is believed to be due to the change of convection velocity of the fluid in the distance perpendicular to the plate. The high amplitude ratio which appears in the inner half of the boundary layer is thought to be the same mechanism as the interaction between a boundary layer and the wake of a stationary circular cylinder which has been studied by Tsiolakis et al (1983).

In conclusion, the phase-averaged velocity and turbulence intensity profiles in a boundary layer which is periodically disturbed by moving wakes have been observed. They are the result of the combination of the moving wake-turbulent boundary layer interaction and the phase lag characteristics. The flow behaviour of the periodically disturbed flat plate boundary layer has also been found to be similar to that measured by Evans (1974) and Hodson (1982) in operating turbomachines. However, this experiment has not considered the effects of pressure gradient and the angle of attack fluctuation in each wake on the downstream blade boundary layer thickness. This effect is also important in correcting the cascade test results of turbomachine blades.

5.2 SUGGESTIONS FOR FURTHER WORK

Further work in this field of study should include the effects of pressure gradient and the fluctuation of angle of attack at the downstream surface. Since the flow in turbomachines is highly turbulent, the boundary layer on blades should be nearly turbulent profiles. The use of longer plate or lower kinematic viscosity fluids are necessary to create fully turbulent boundary layers.

No calculation procedure has been found to describe the behaviour of a boundary layer in a free stream which is disturbed by periodic traversing wakes. Analytical or numerical procedures must be developed to compare with experimental data, such as those obtained here and in the future.

FIGURES

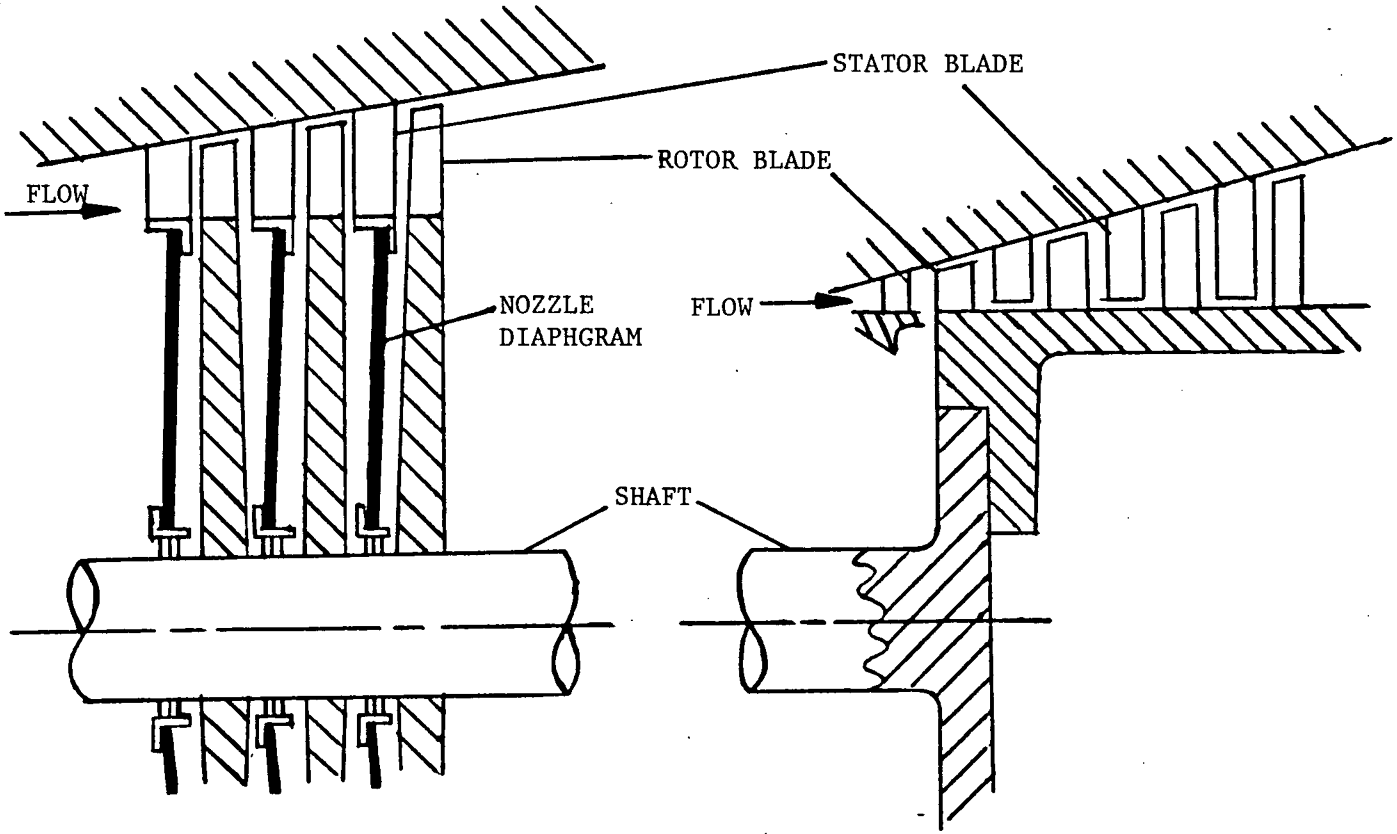

a) DISK

b) DRUM

Fig.1.1 TWO COMMON CONSTRUCTIONS OF AXIAL FLOW TURBINES

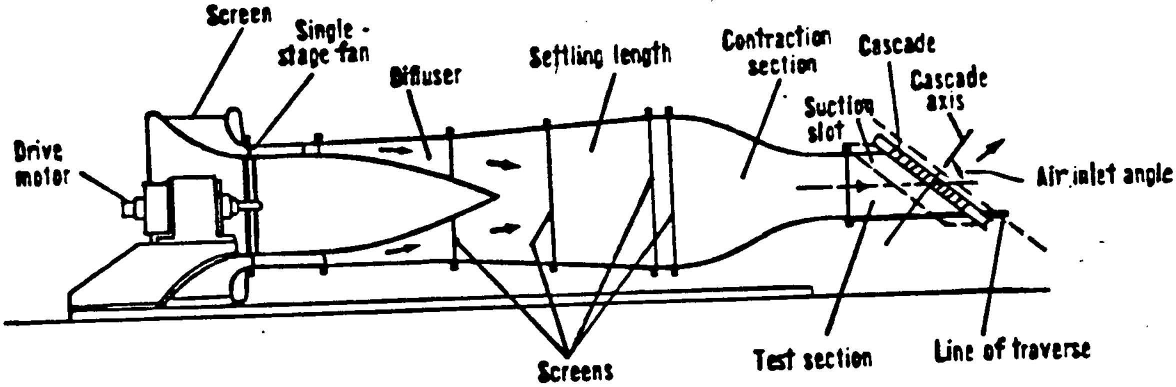

Fig.1.2 LAYOUT OF A CONVENTIONAL LOW SPEED CASCADE TUNNEL (DIXON 1978)

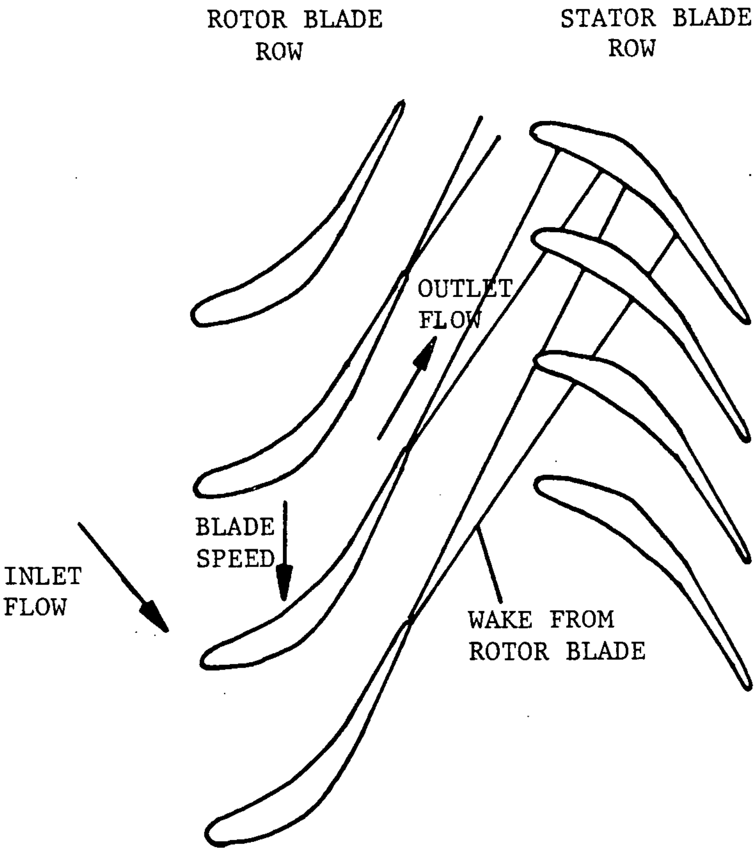

Fig. 1.3 SCHEMATIC DIAGRAM OF PERIODIC DISTURBANCE ON TURBINE STATOR BLADES

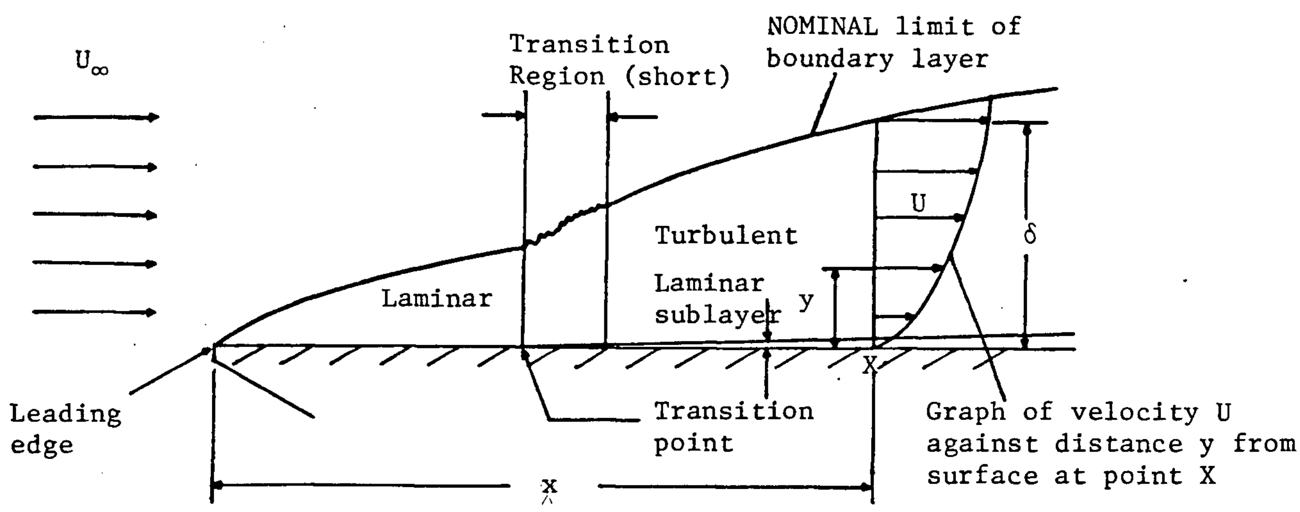

FIG.2.1 SCHEMATIC DIAGRAM OF FLAT PLATE BOUNDARY LAYER DEVELOPMENT (MASSEY 1968)

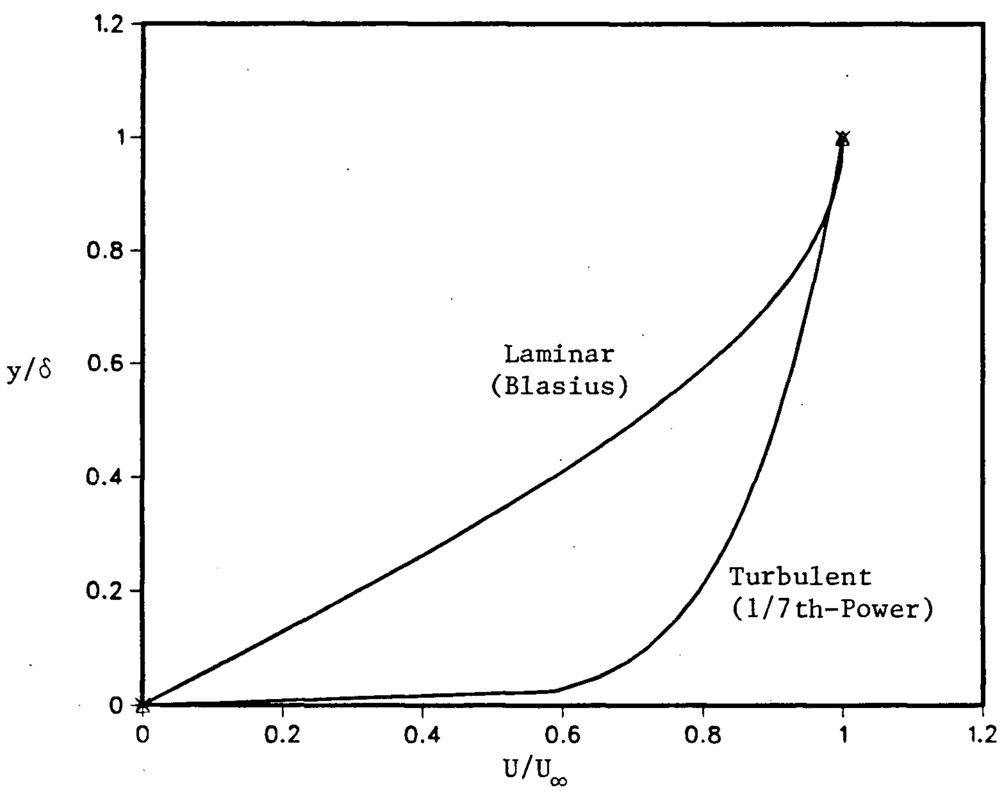

FIG.2.2 TYPICAL DISTRIBUTIONS IN LAMINAR AND TURBULENT BOUNDARY LAYERS ON A FLAT PLATE

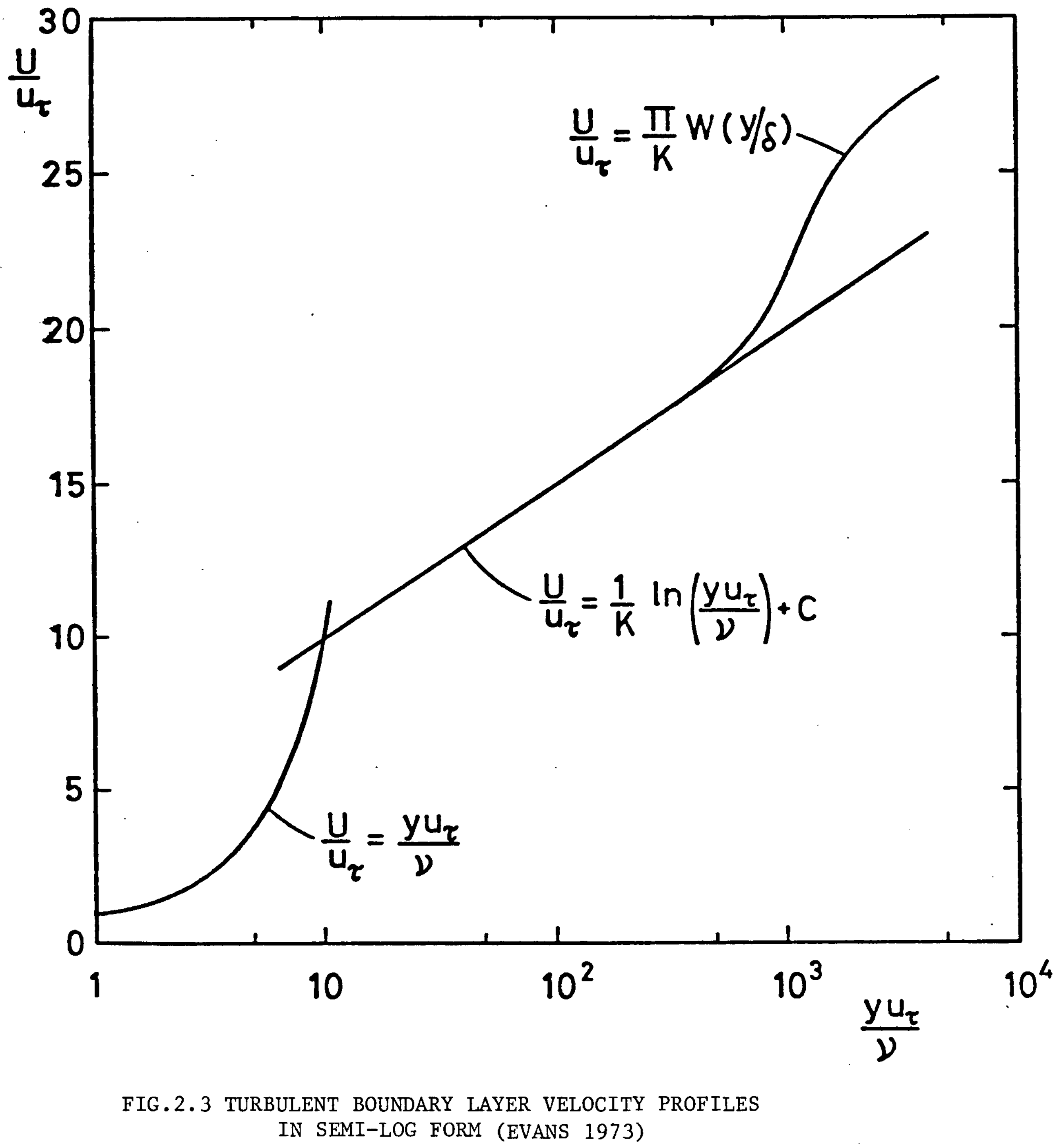

FIG.2.3 TURBULENT BOUNDARY LAYER VELOCITY PROFILES
IN SEMI-LOG FORM (EVANS 1973)

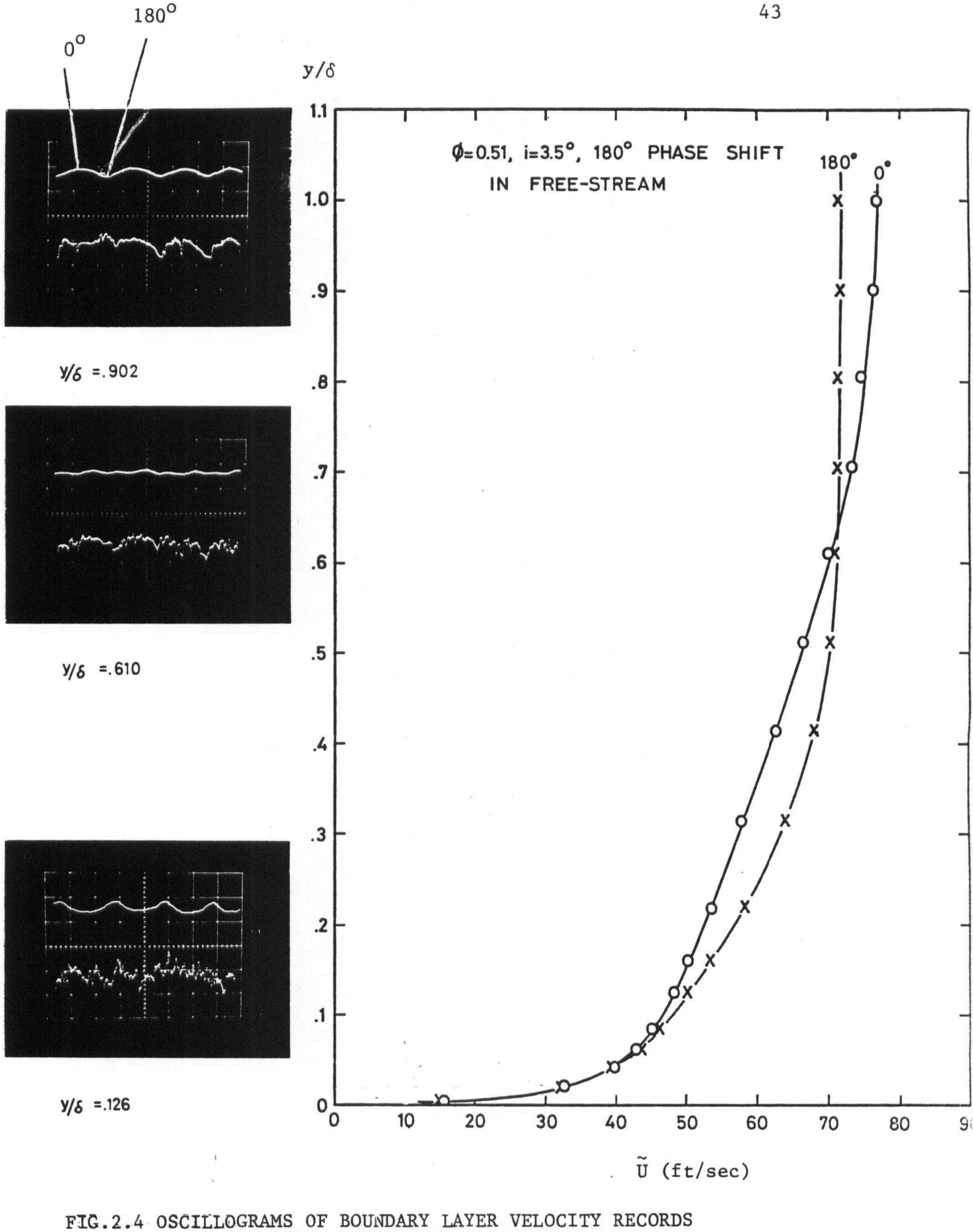

FIG.2.4 OSCILLOGRAMS OF BOUNDARY LAYER VELOCITY RECORDS
AND INSTANTANEOUS VELOCITY PROFILES
ON A COMPRESSOR STATOR BLADE, x/C=0.5 (EVANS 1977)

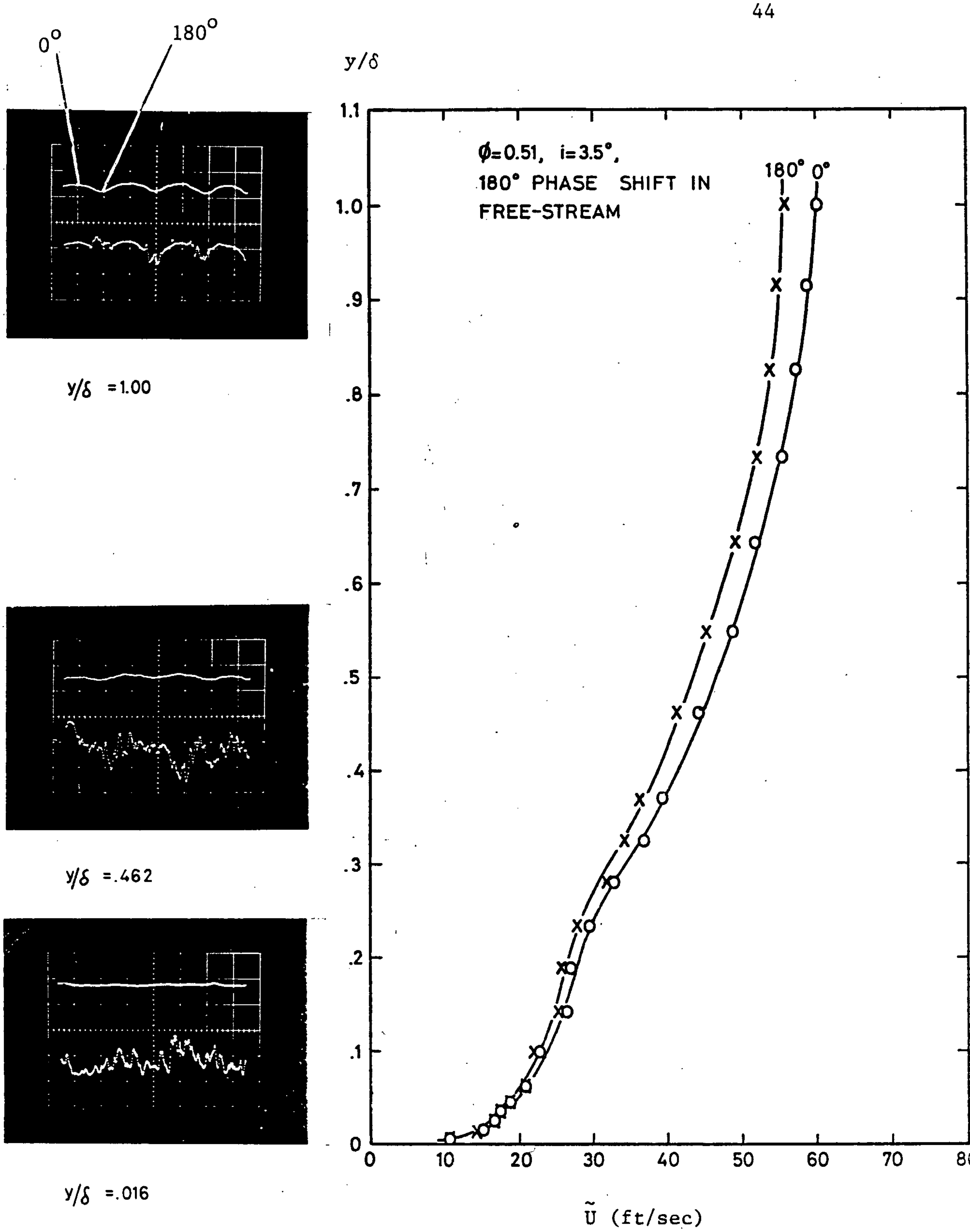

FIG.2.5 OSCILLOGRAMS OF BOUNDARY LAYER VELOCITY RECORDS AND INSTANTANEOUS VELOCITY PROFILES ON A COMPRESSOR STATOR BLADE, x/C=0.7 (EVANS 1977)

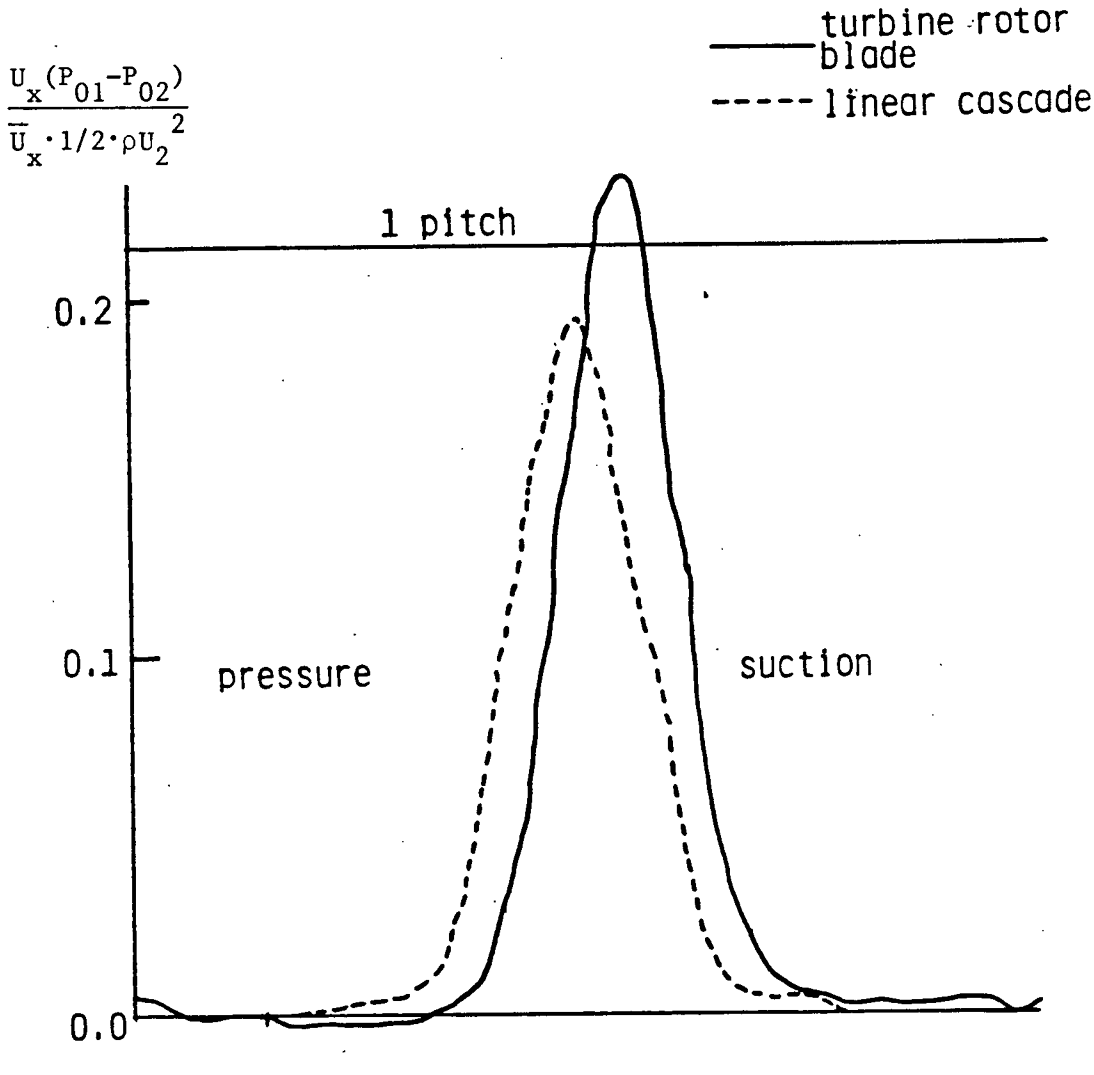

FIG.2.6 PRESSURE LOSS COEFFICIENTS ACROSS A TURBINE ROTOR BLADE AND THE SAME BLADE IN A LINEAR CASCADE (HODSON 1983)

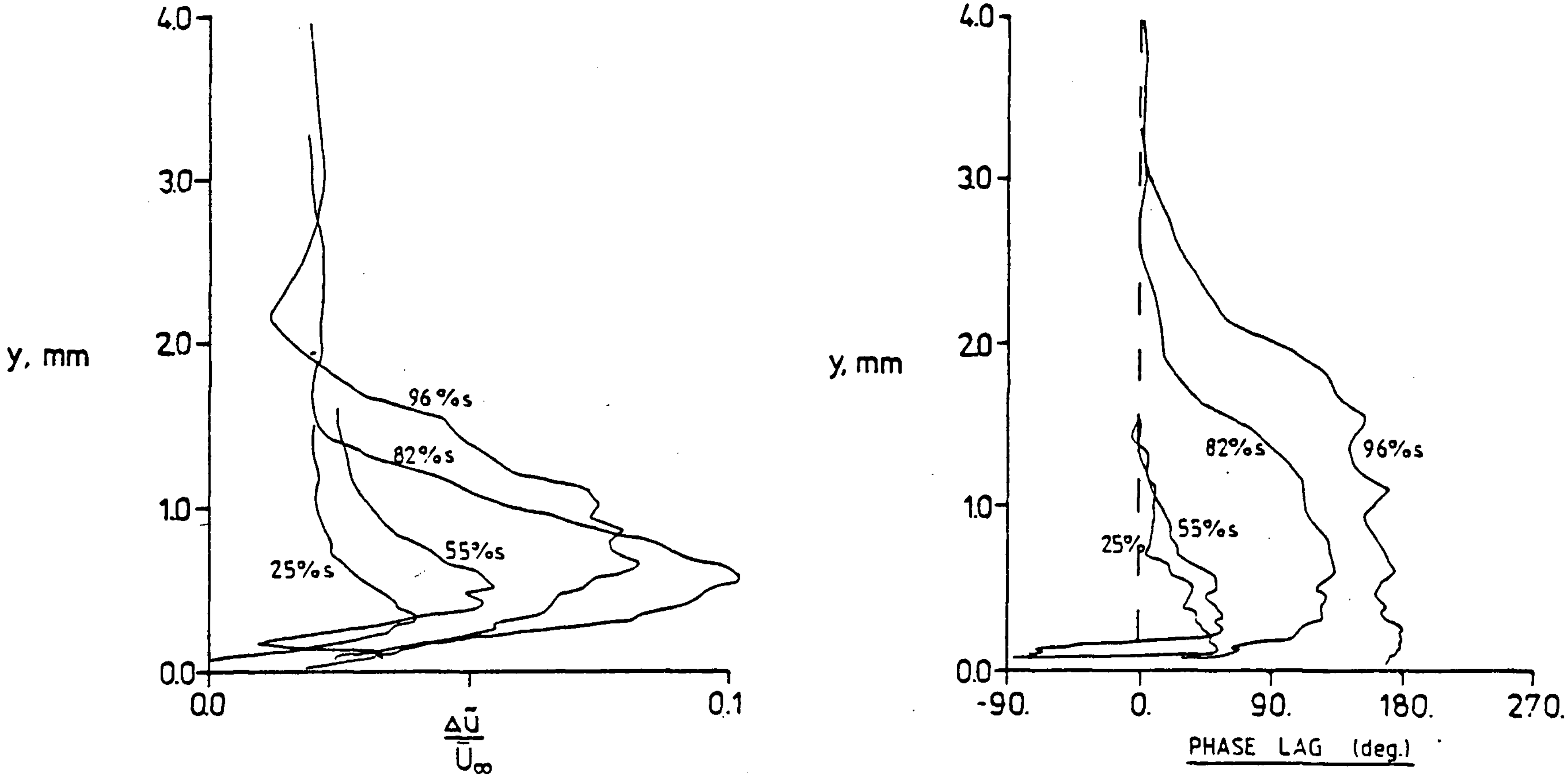

FIG. 2.7 AMPLITUDE AND PHASE PROFILES FOR THE BOUNDARY LAYERS OF A TURBINE ROTOR BLADE SUCTION-SURFACE (HODSON 1983)

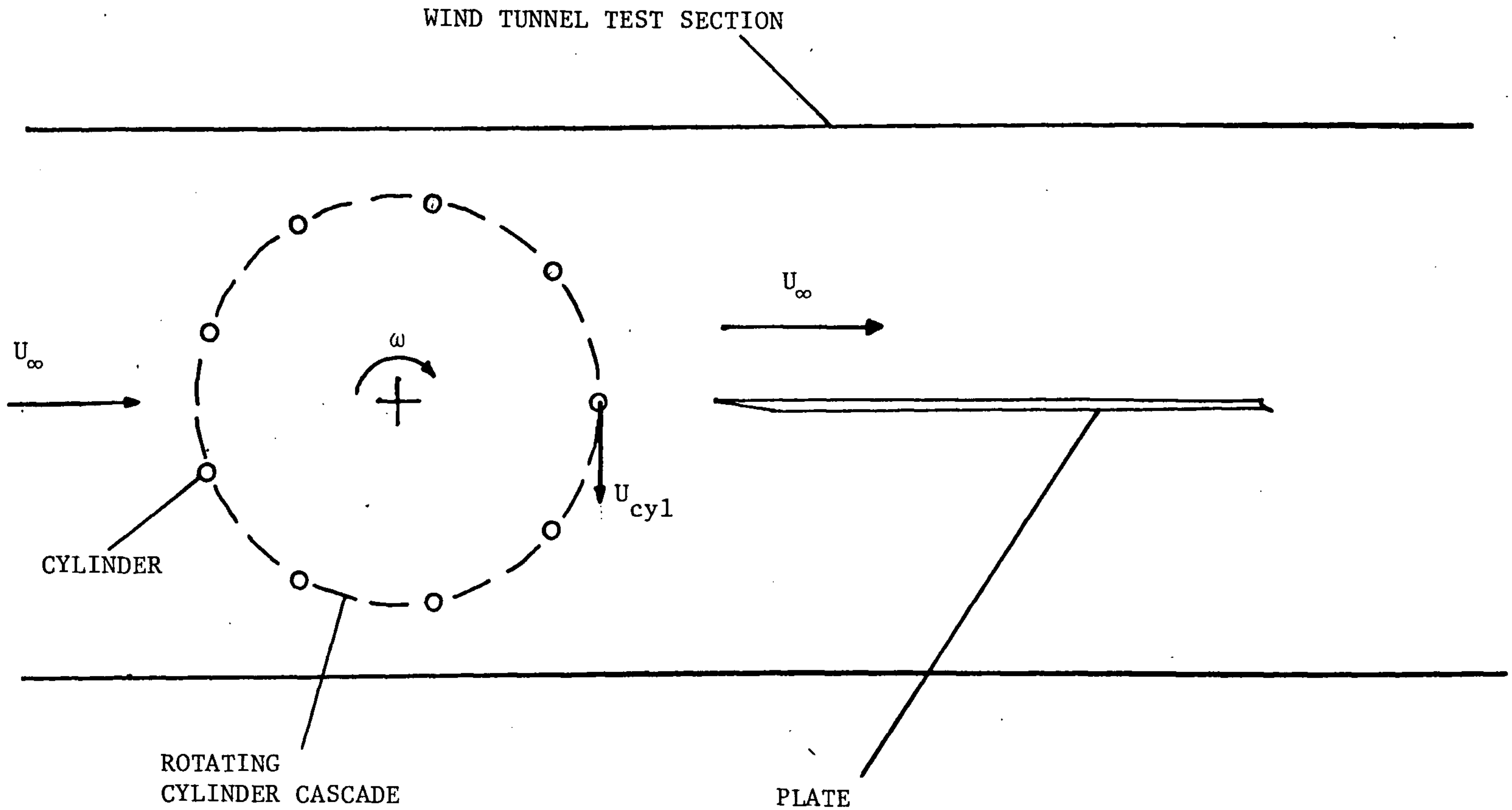

FIG.2.8 SCHEMATIC DIAGRAM OF EXPERIMENTAL SET UP USED BY PFEIL, HERBST AND SCHRODER (1982)

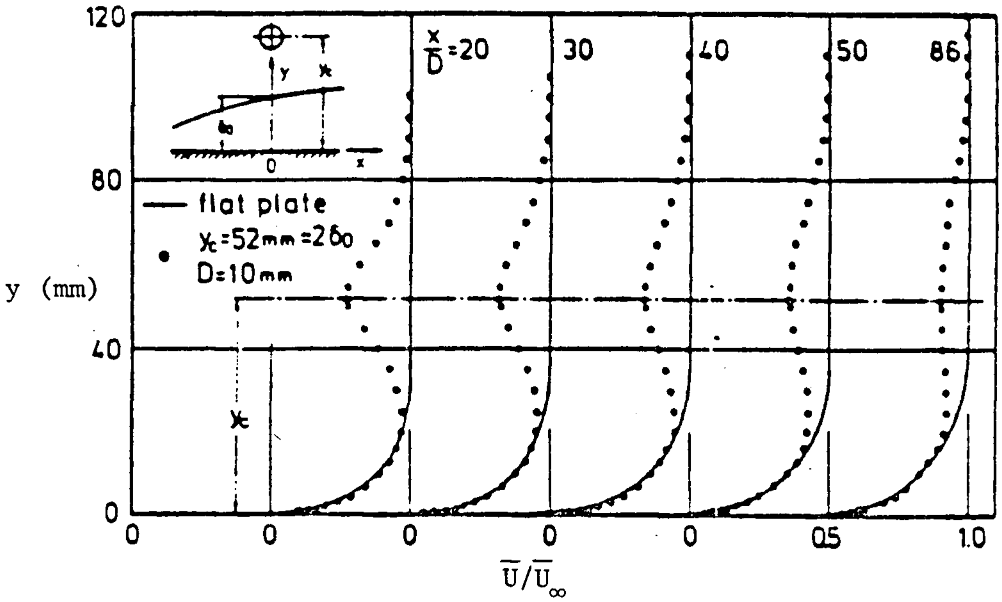

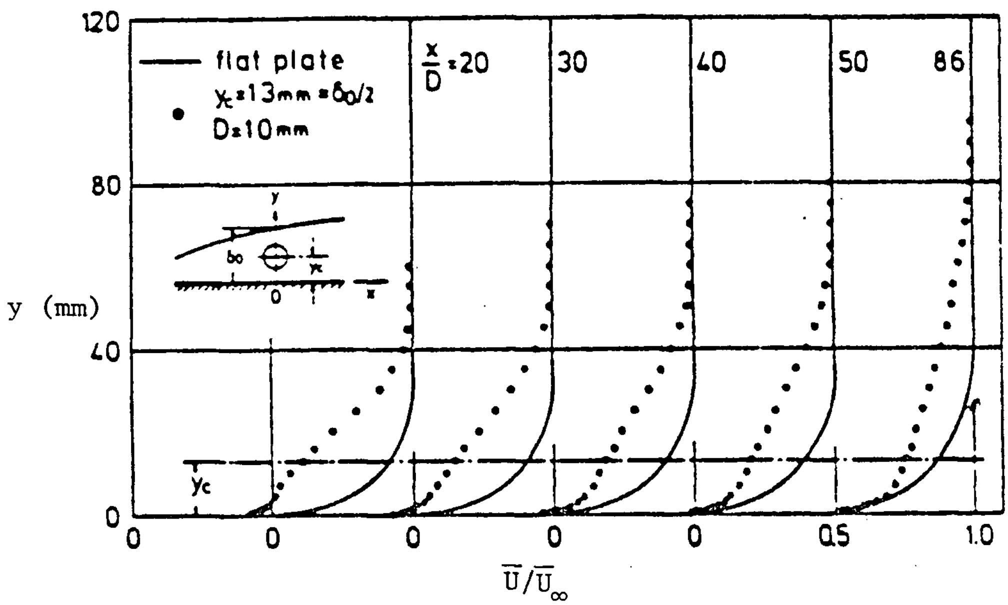

FIG.2.9 MEASURED MEAN VELOCITIES OF WAKE AND BOUNDARY LAYER INTERACTING FLOW (......) COMPARED TO UNDISTURBED, FLAT PLATE FLOW (———)
(TSIOLAKIS, KRAUSE AND MULLER 1983)

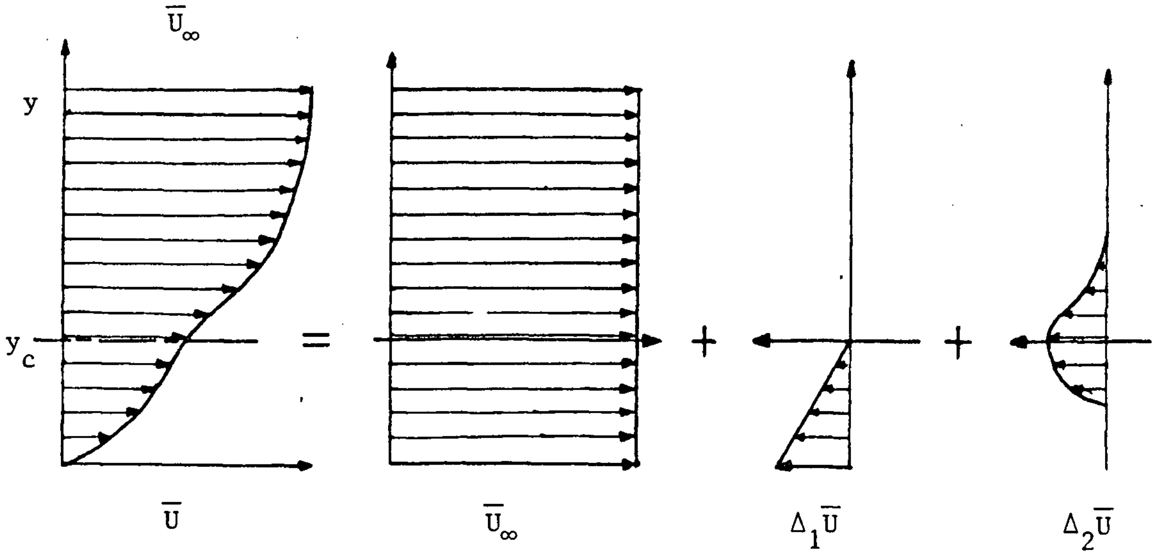

FIG. 2.10 DECOMPOSITION OF BOUNDARY LAYER-WAKE INTERACTION FOR ANALYZING SELF-SIMILARITY OF WAKE FLOW (TSIOLAKIS, KRAUSE AND MULLER 1983)

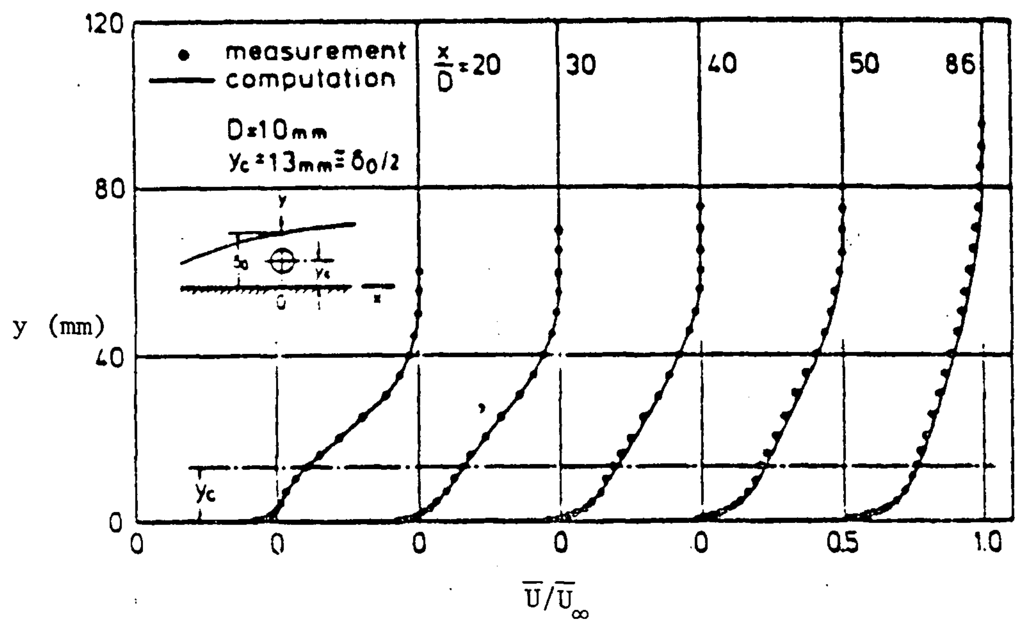

FIG.2.11 COMPARISON OF MEASURED MEAN VELOCITIES WITH RESULTS OF FINITE-DIFFERENCE SOLUTION (TSIOLAKIS, KRAUSE AND MULLER 1983)

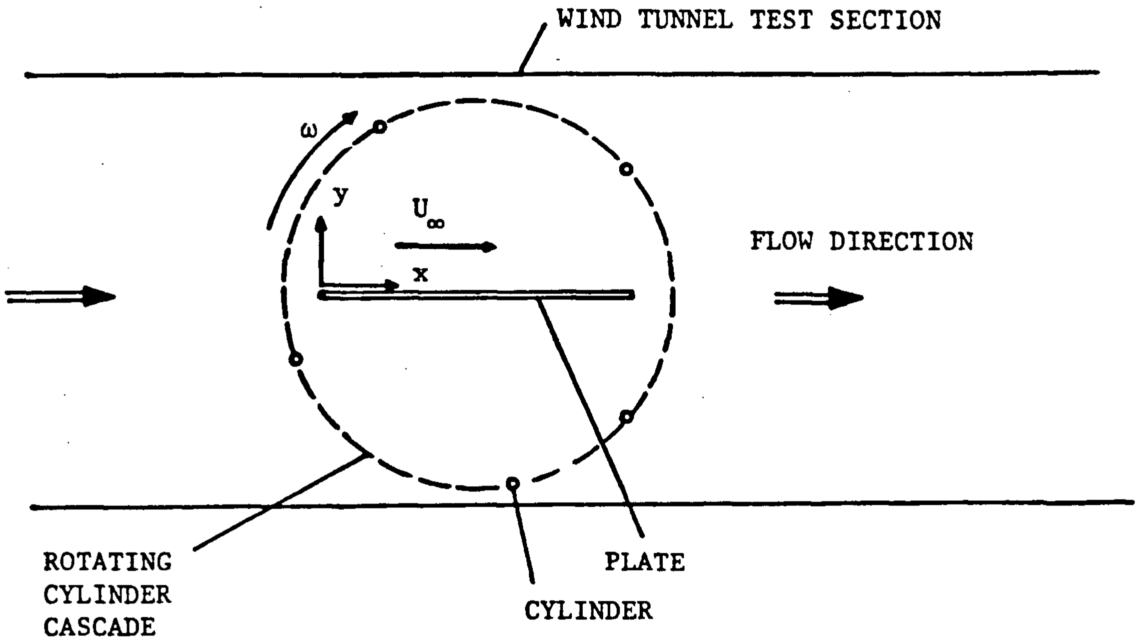

FIG.3.1 SCHEMATIC DIAGRAM OF THE EXPERIMENTAL SET-UP USED IN THIS STUDY

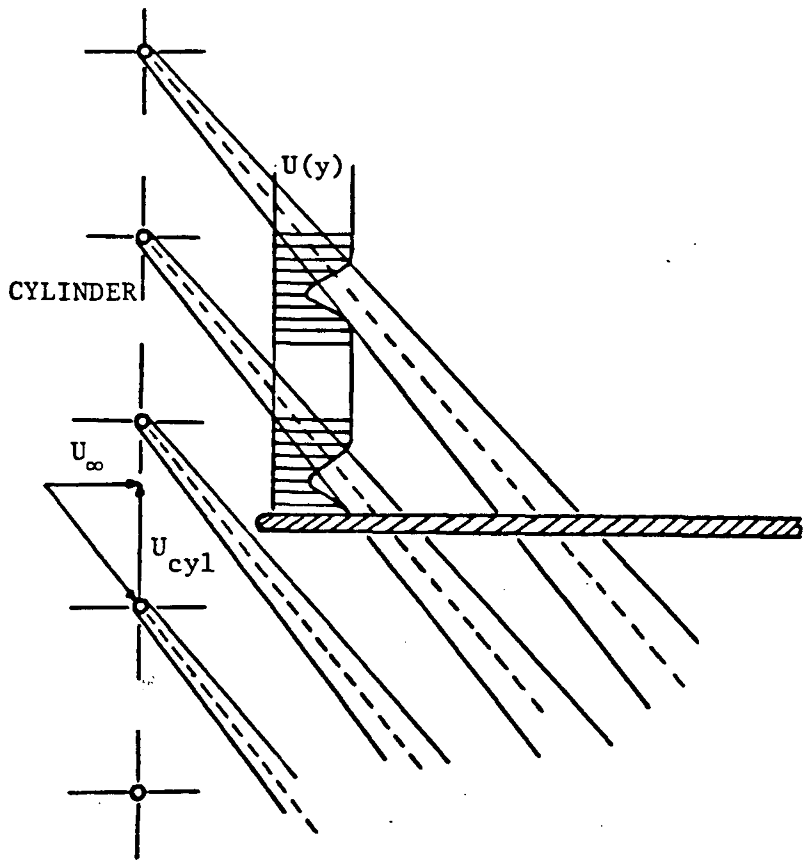

FIG. 3.2 SCHEMATIC DIAGRAM OF THE UNSTEADY FLOW PRODUCED BY WAKES

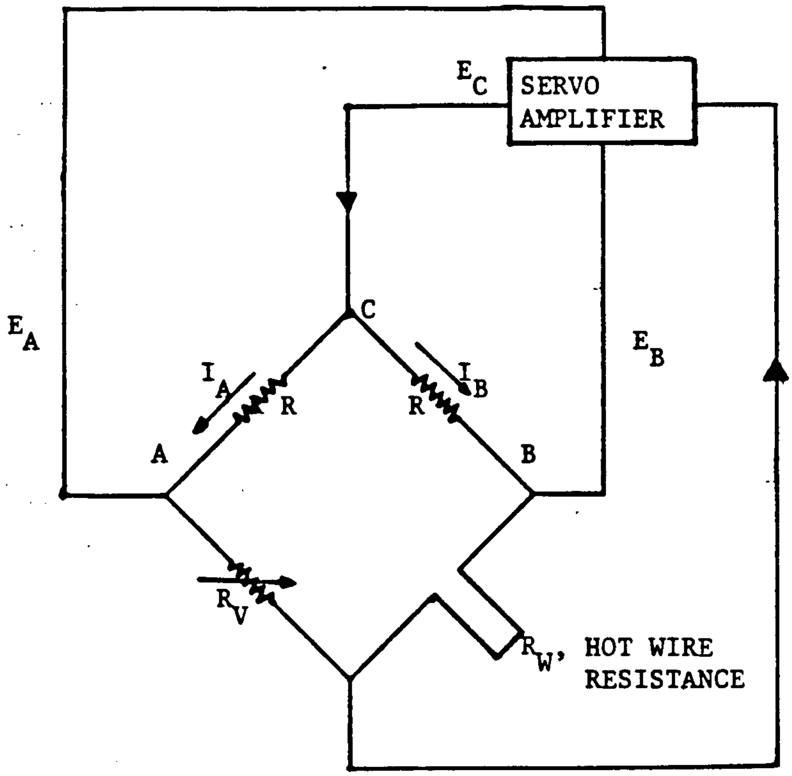

FIG. 3.3 TYPICAL CONSTANT TEMPERATURE HOT WIRE ANEMOMETER BRIDGE

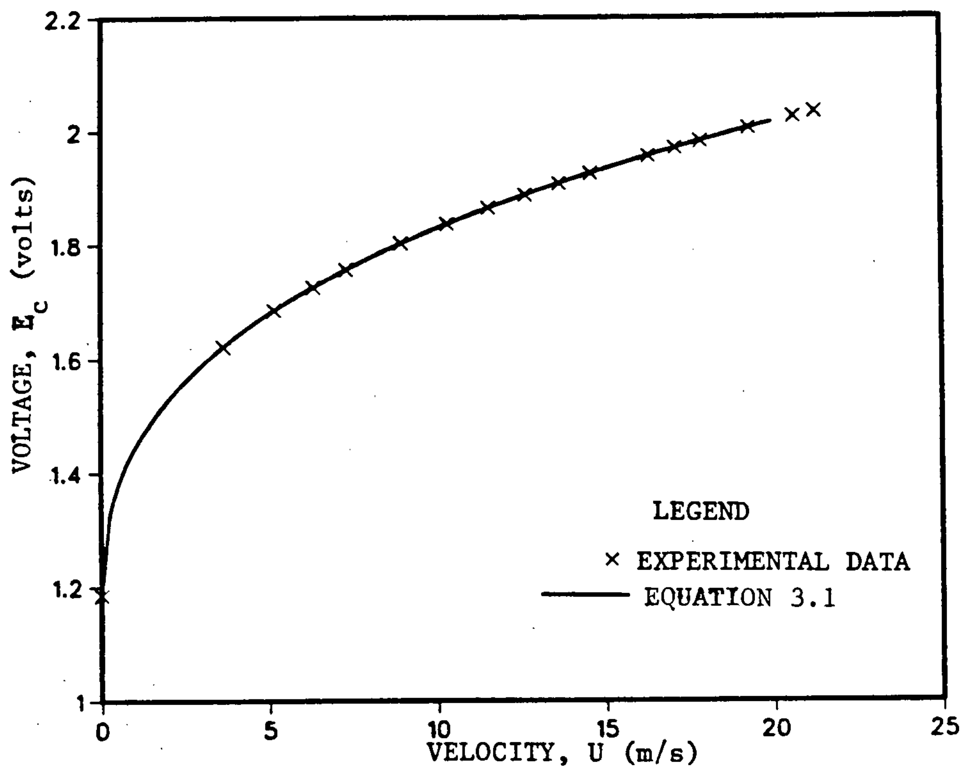

FIG. 3.4 CALIBRATION CURVE OF THE CONSTANT TEMPERATURE HOT WIRE ANEMOMETER

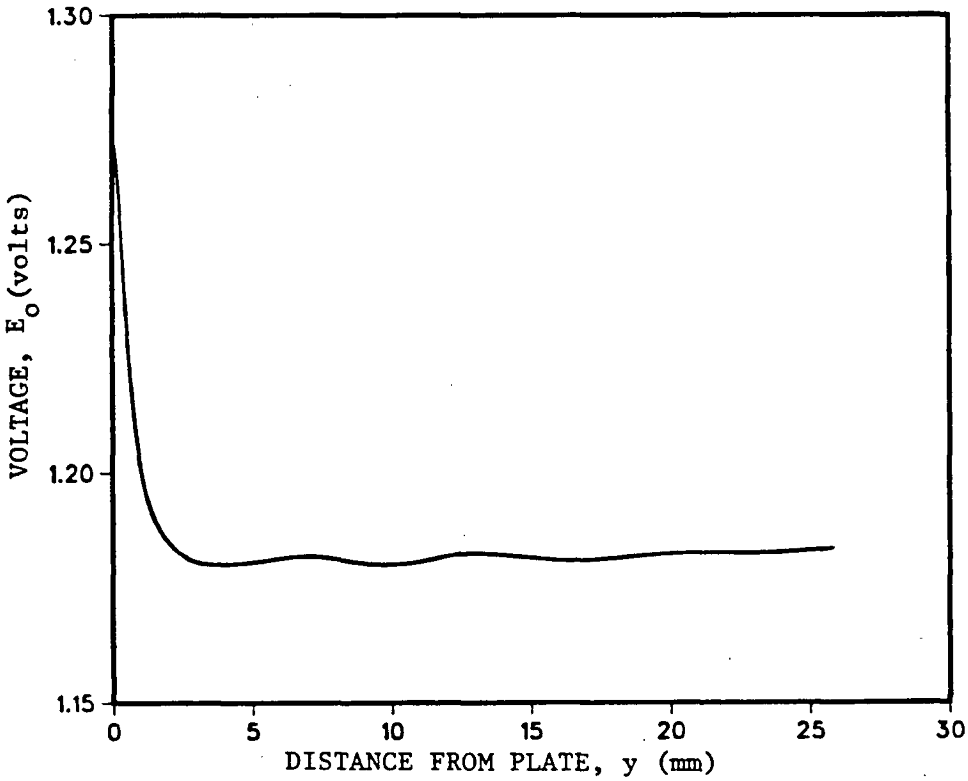

FIG. 3.5 STILL AIR WALL CORRECTION FOR HOT WIRE ANEMOMETER

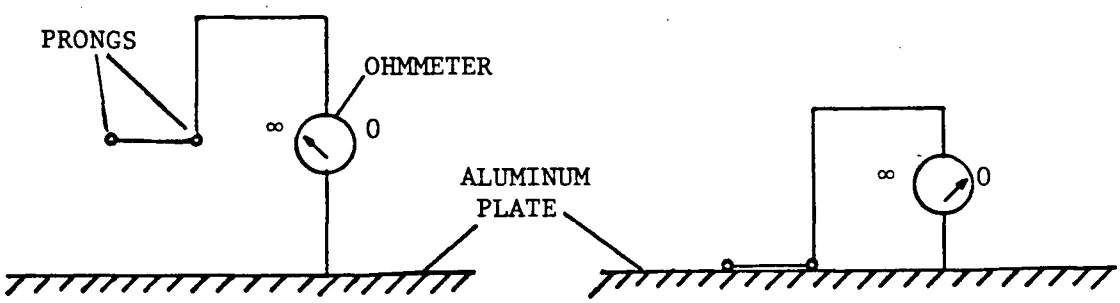

FIG. 3.6 METHOD OF DETECTING THE CONTACT OF THE HOT WIRE PROBE AND THE ALUMINUM FLAT PLATE

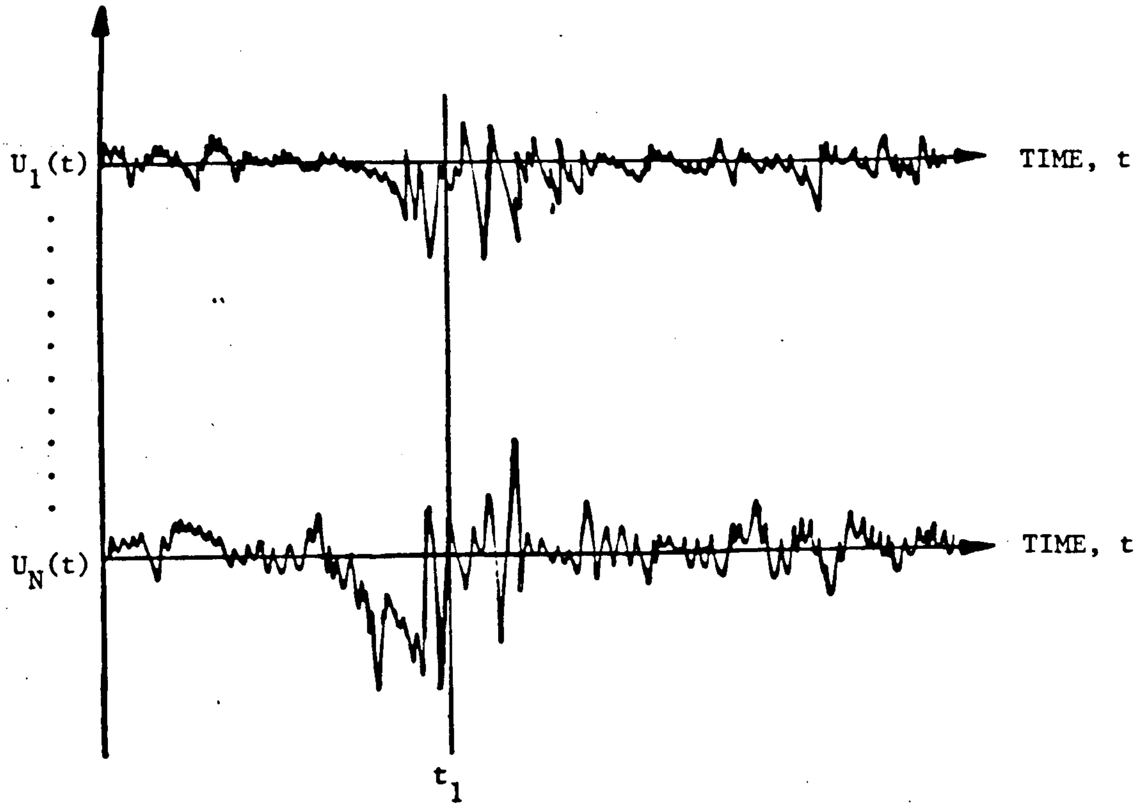

a) TYPICAL VELOCITY RECORDS AT ONE LOCATION STARTING AT THE SAME INSTANT OF TIME

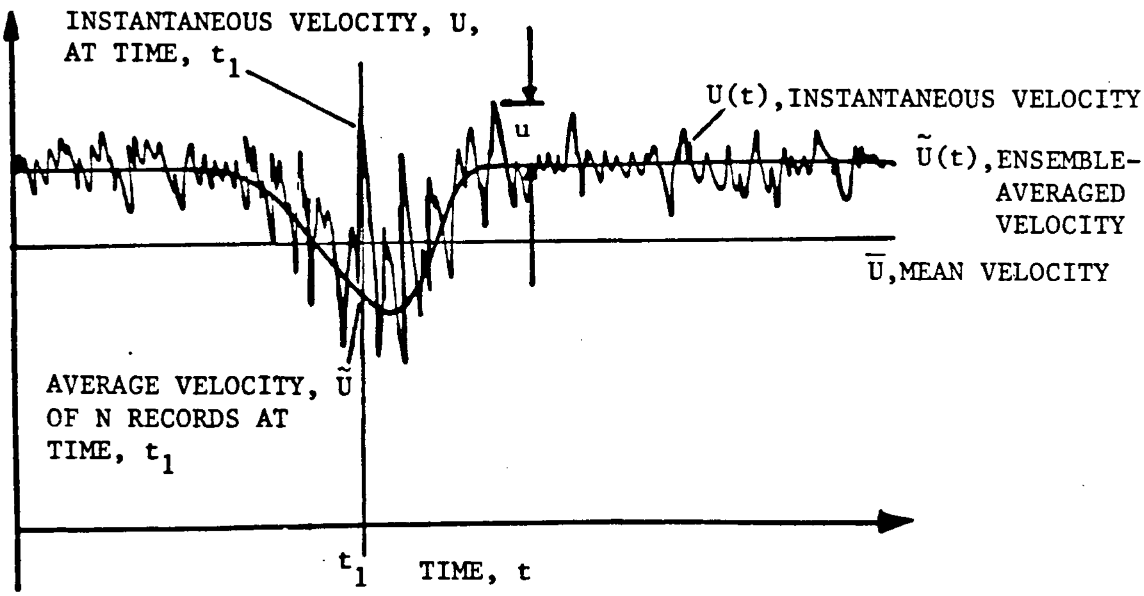

b) TYPICAL ENSEMBLE-AVERAGED VELOCITY RECORD

FIG. 3.7 AN ILLUSTRATION OF THE ENSEMBLE AVERAGING PROCEDURE

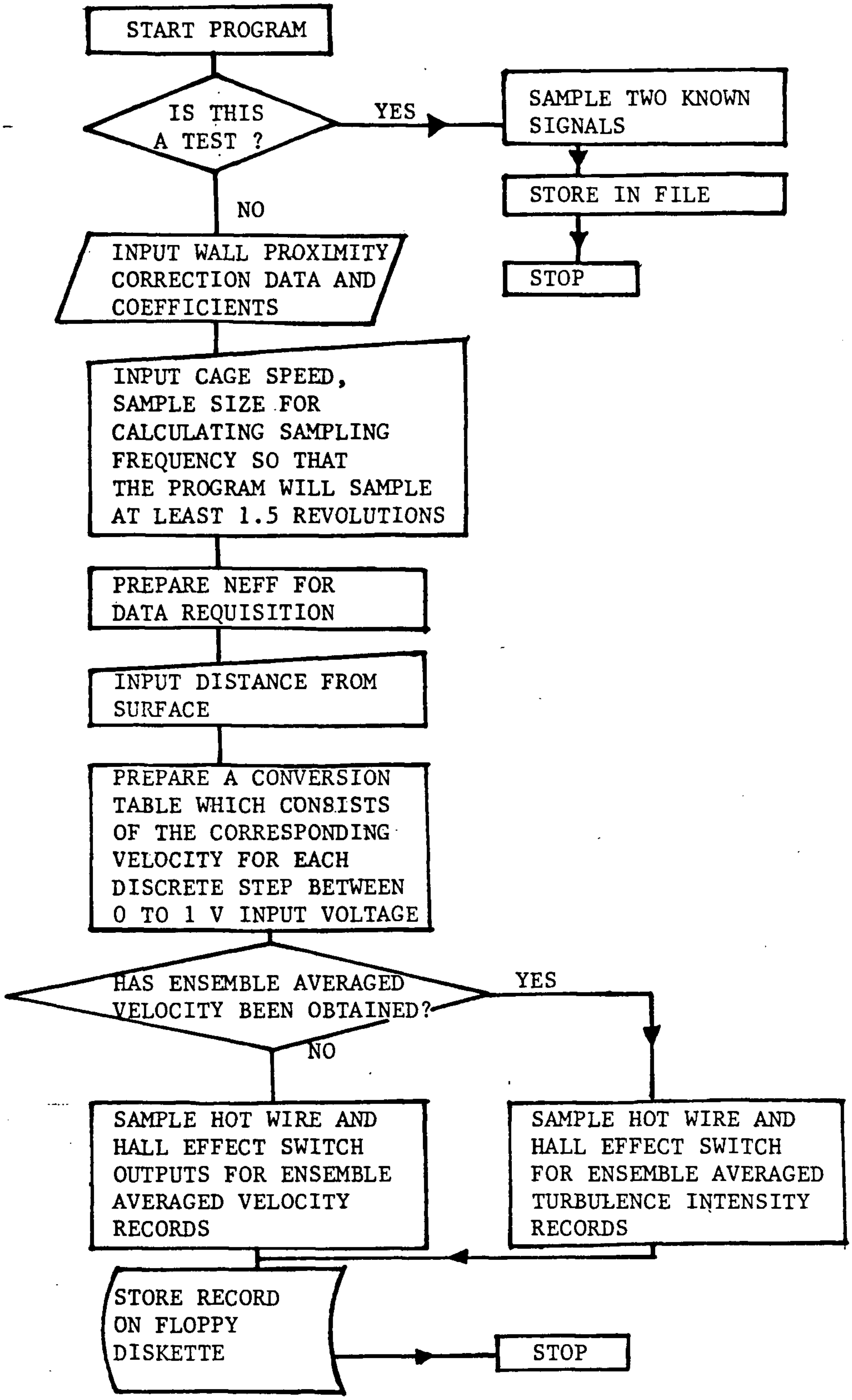

FIG. 3.8 DATA ACQUISITION PROGRAM FLOW CHART

PLATE 1 THE LOW SPEED WIND TUNNEL

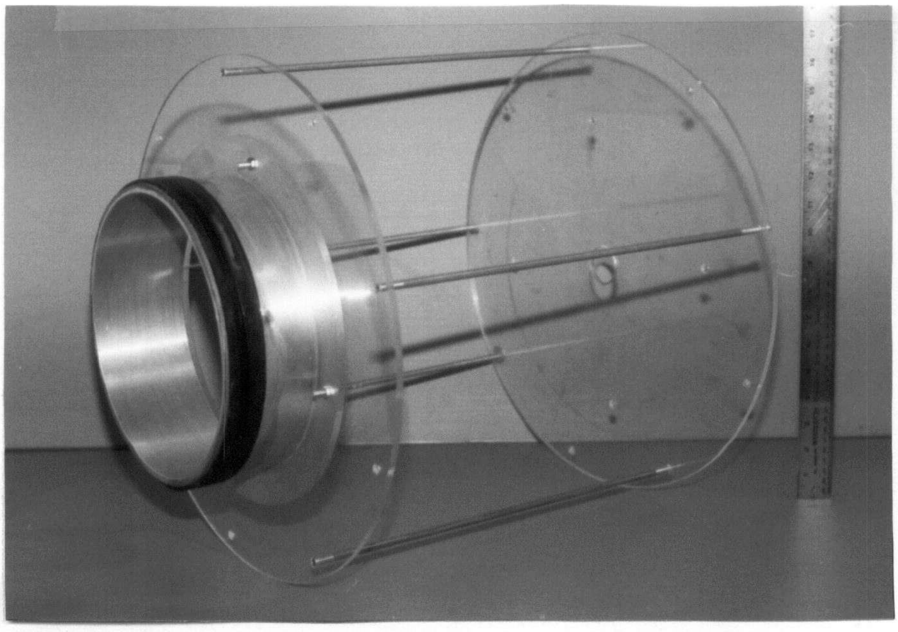

PLATE 2 THE CYLINDER CASCADE

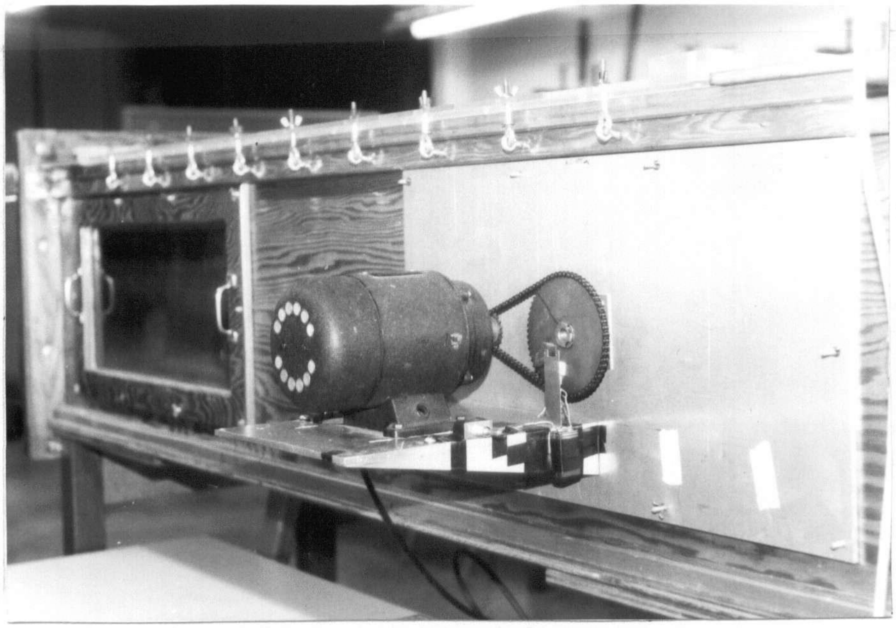

PLATE 3 THE DRIVING MOTOR AND SPEED REDUCTION GEARS

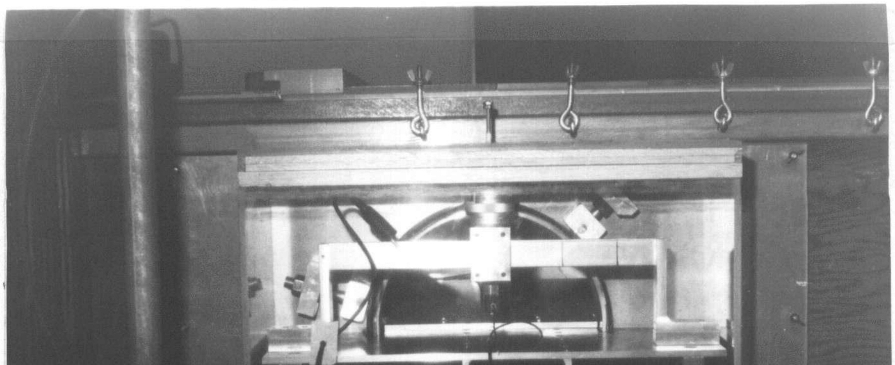

PLATE 4 BEARINGS AND THE TRAVERSE MECHANISM

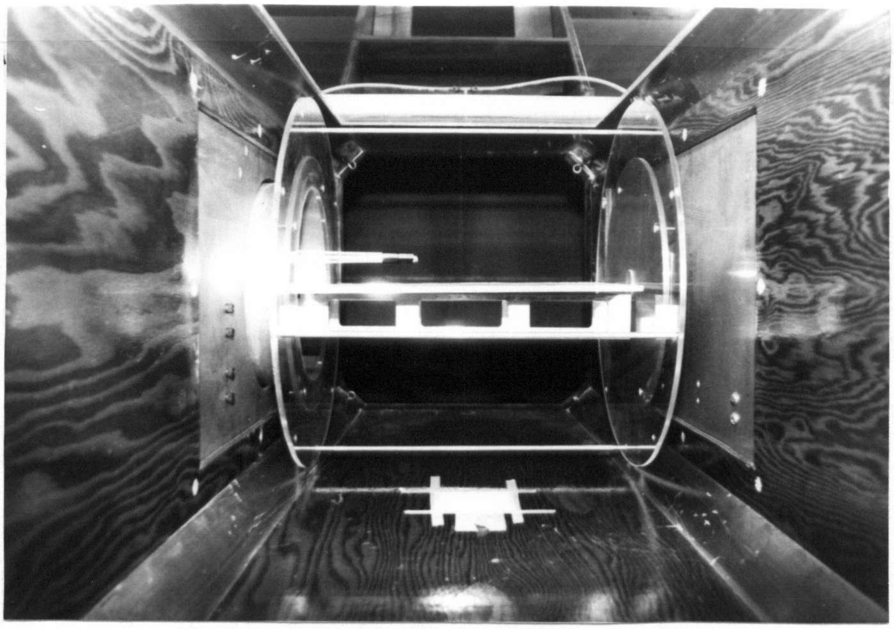

PLATE 5 THE FLAT PLATE AND SUPPORT

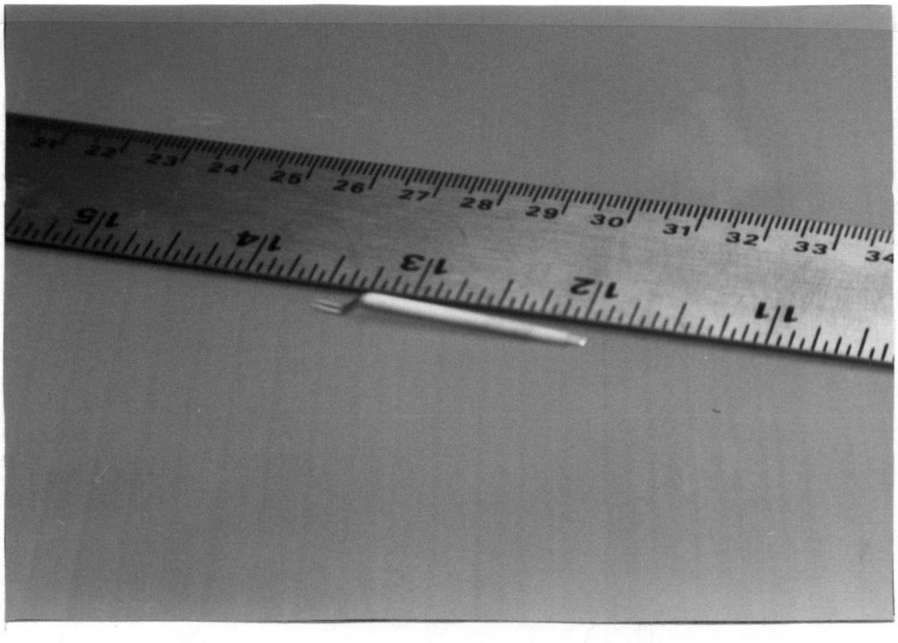

PLATE 6 THE HOT WIRE PROBE FOR BOUNDARY LAYER MEASUREMENT

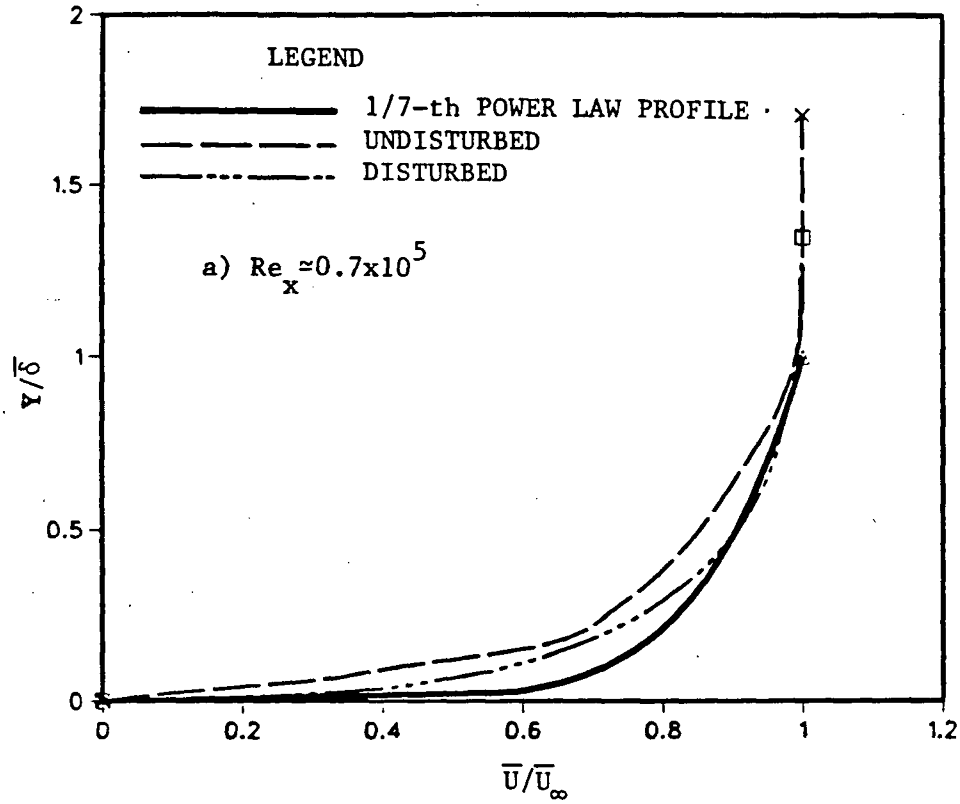

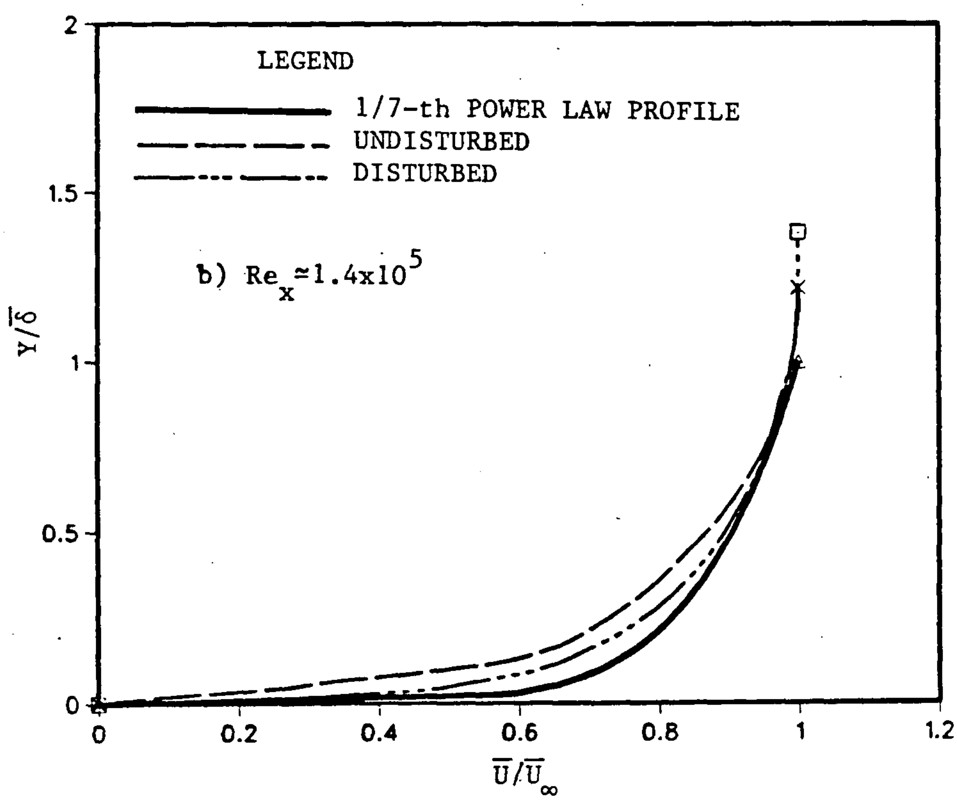

FIG. 4.1a&b NONDIMENSIONAL TIME AVERAGED VELOCITY PROFILES, $C_\phi = 0.84$, $\omega = 50Hz$

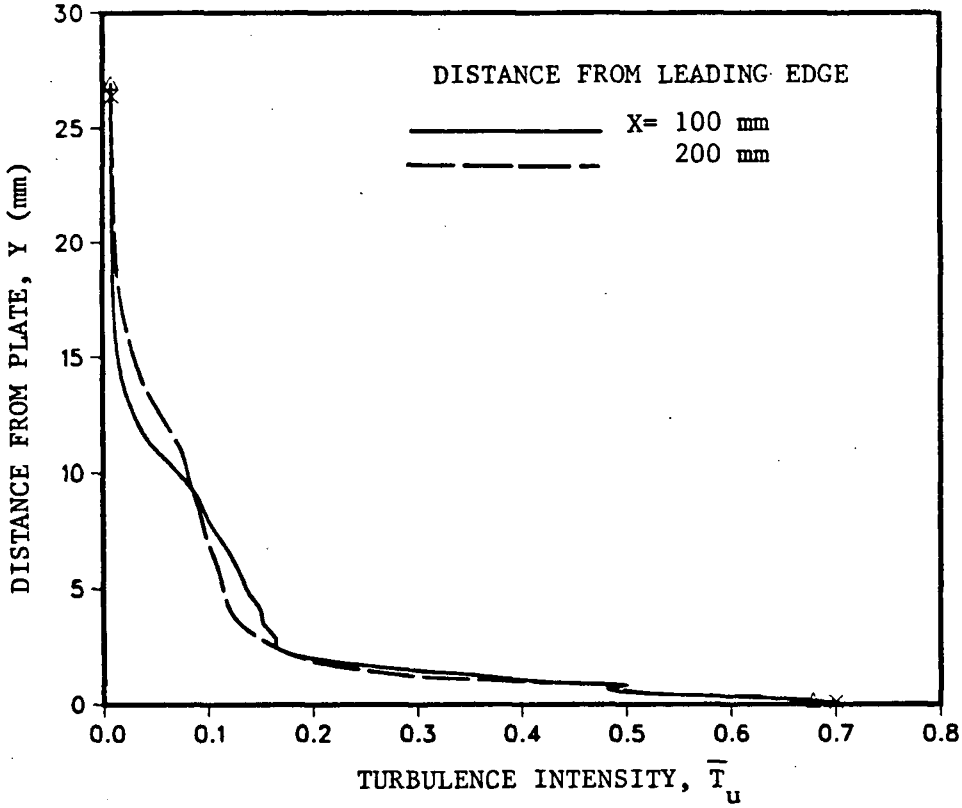

FIG. 4.2 DIMENSIONAL TURBULENCE INTENSITY PROFILES OF UNDISTURBED BOUNDARY LAYER, $\overline{U}_\infty$= 11.75 m/s

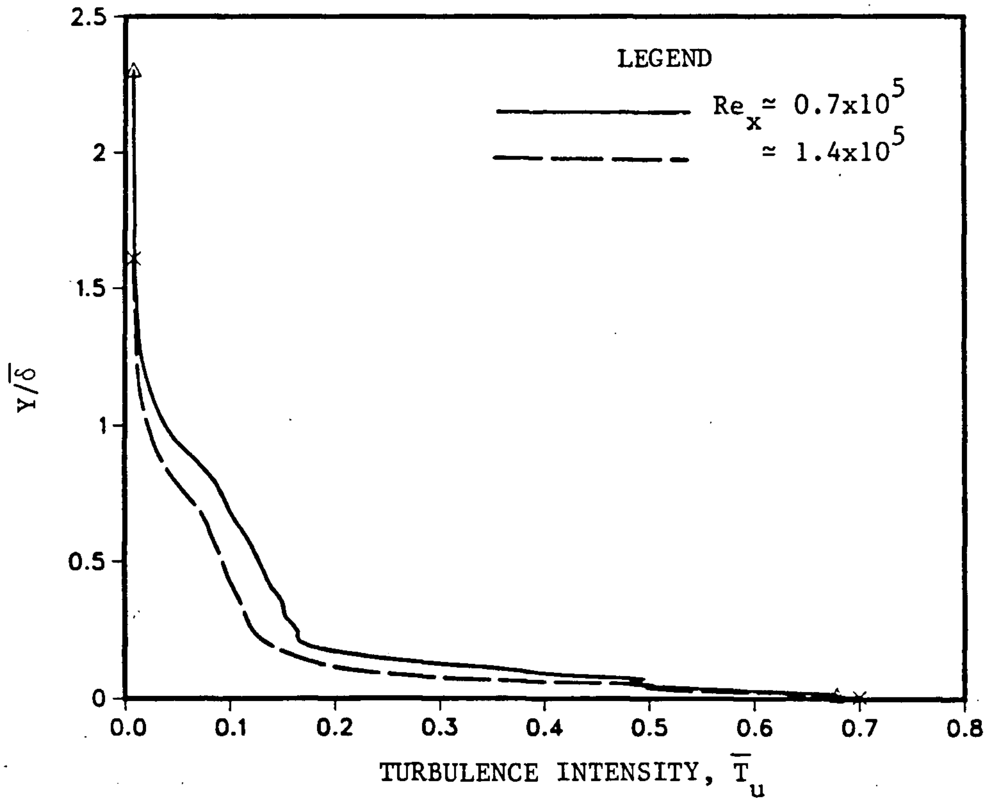

FIG. 4.3 NONDIMENSIONAL TURBULENCE INTENSITY PROFILES OF UNDISTURBED BOUNDARY LAYER

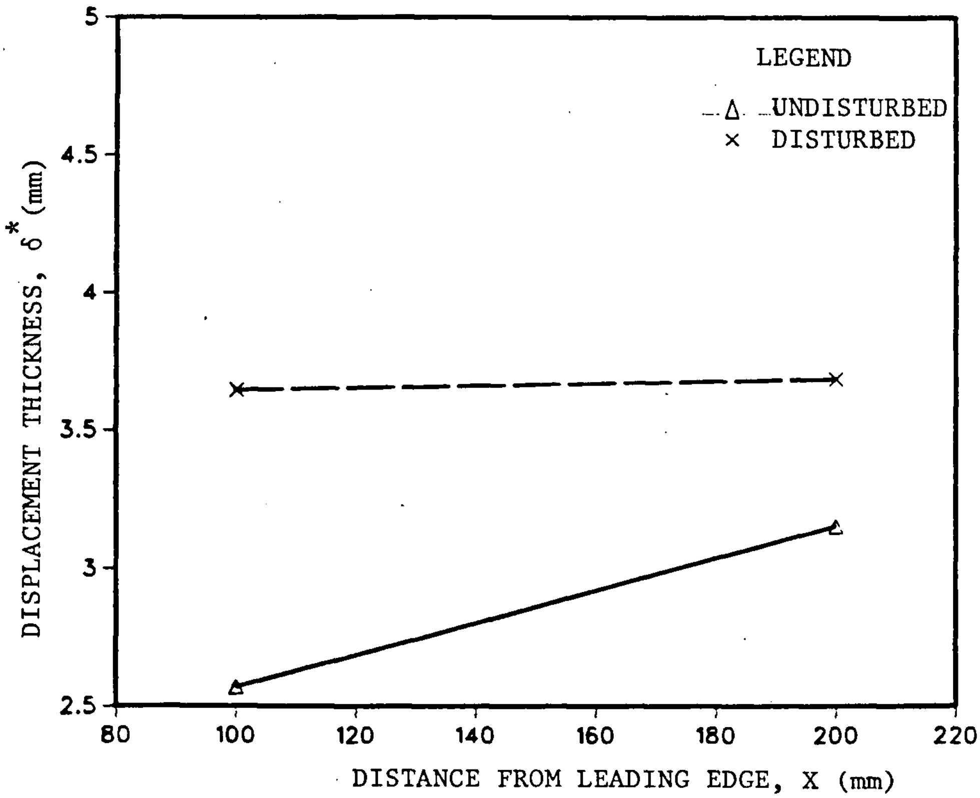

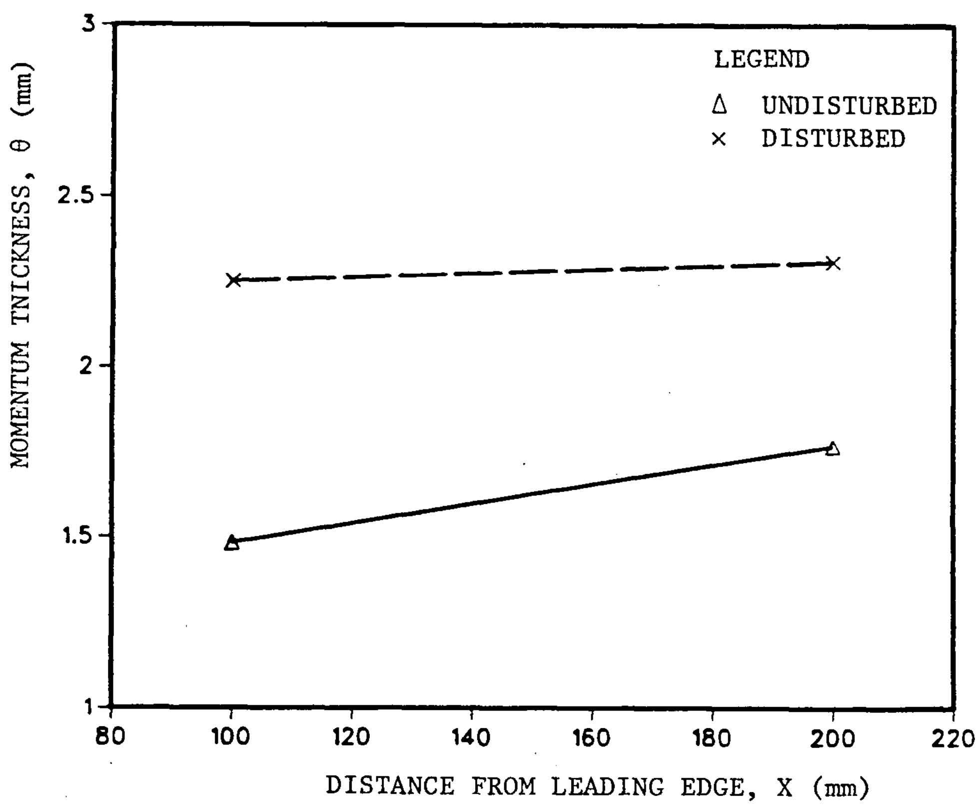

FIG. 4.4 BOUNDARY LAYER DEVELOPMENT, $C_\phi = 0.84$, $\omega = 50Hz$

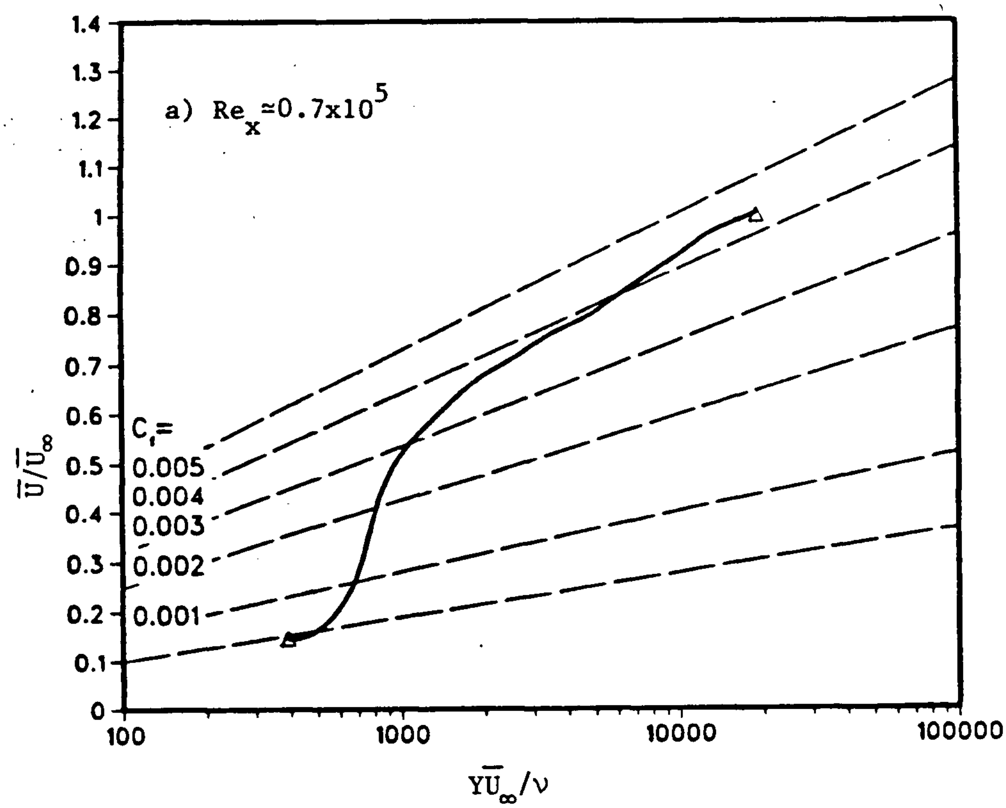

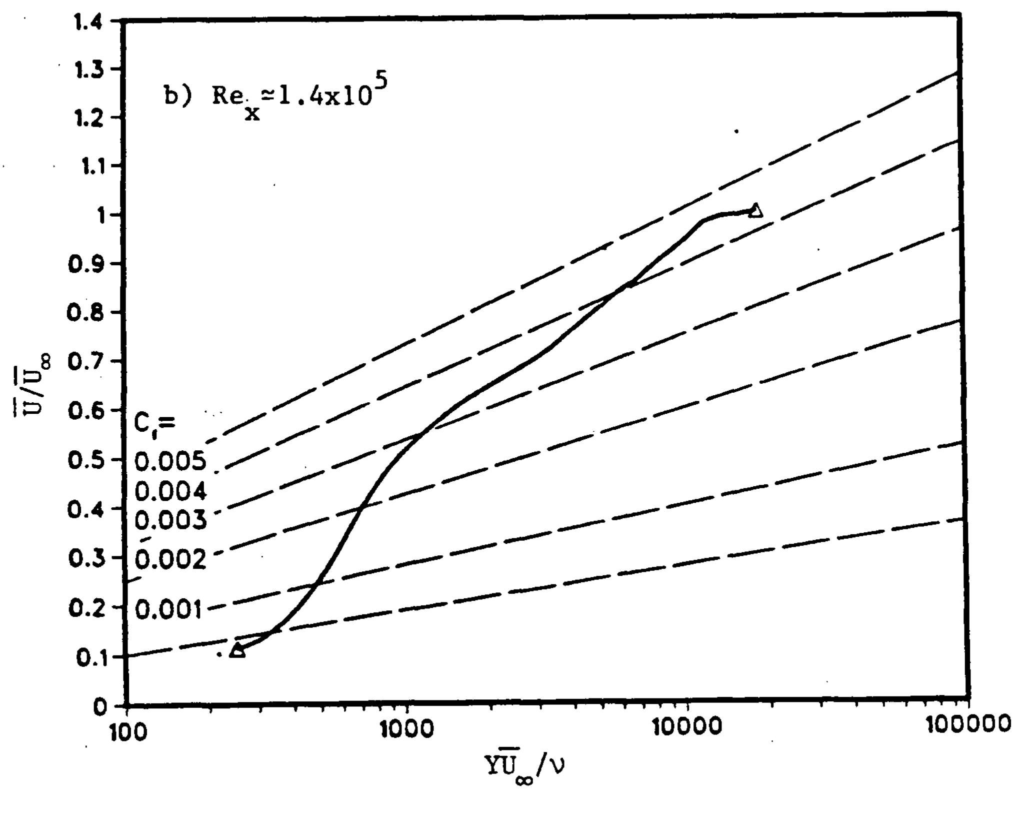

FIG. 4.5a&b CLAUSER PLOTS OF TIME AVERAGED VELOCITY PROFILES OF DISTURBED BOUNDARY LAYERS, C_ϕ=0.84, ω=50 Hz

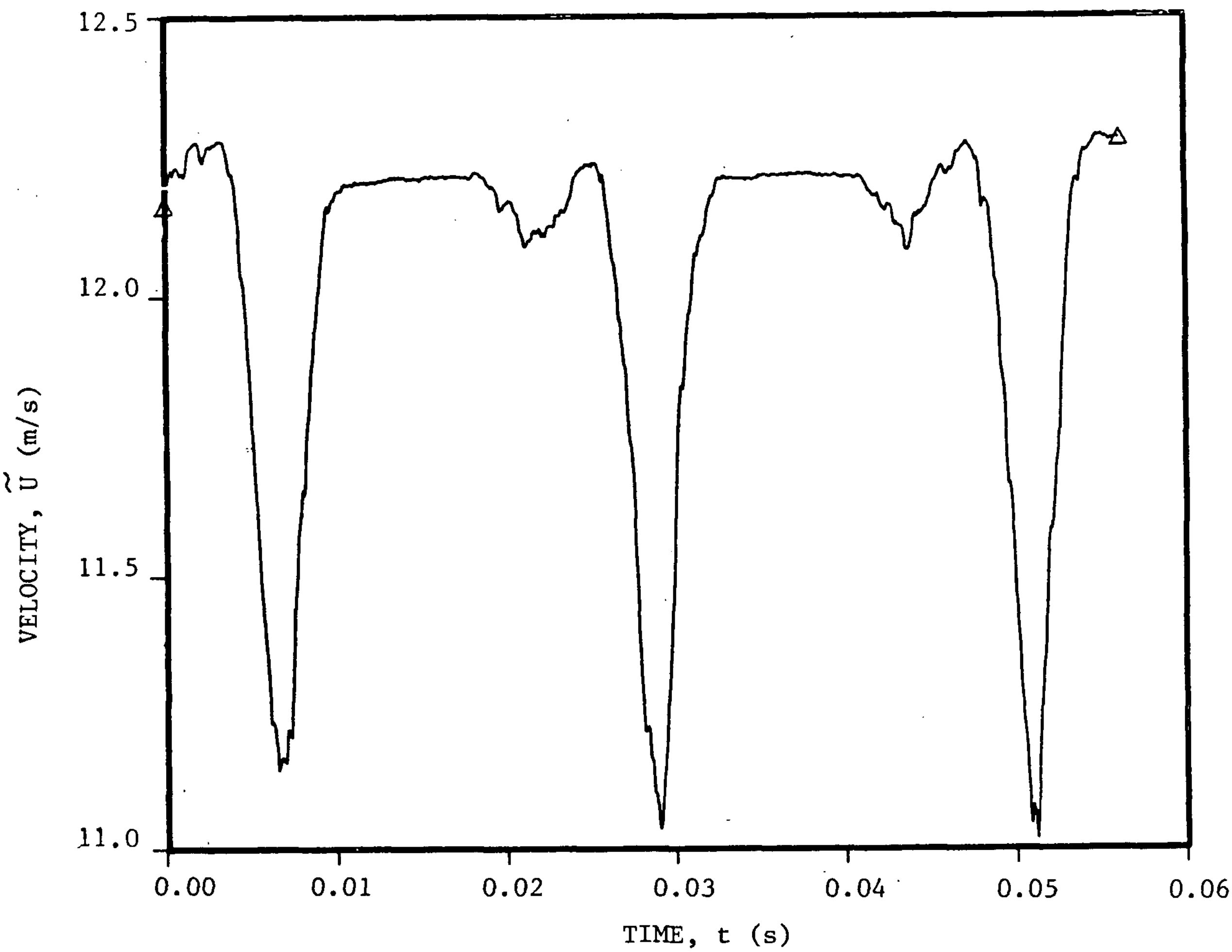

FIG. 4.6 ENSEMBLE-AVERAGED TIME-VELOCITY RECORD OF A TRAVERSING WAKE AT $\overline{U}_{\infty}$= 11.75 m/s, U_B= 14 m/s AND X_o= 26 cm

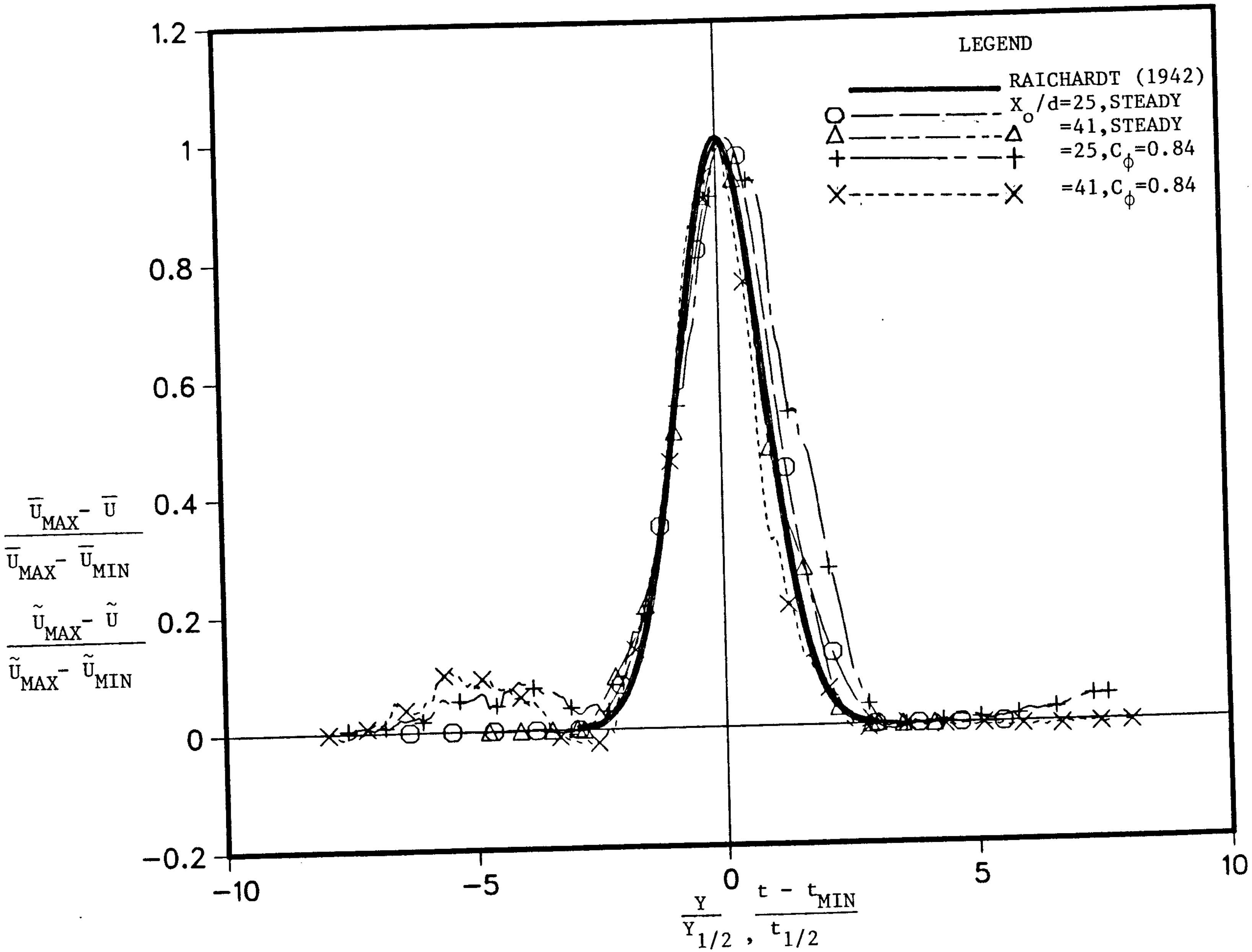

FIG. 4.7 NONDIMENSIONAL WAKE VELOCITY PROFILES
$Re_d \approx 5000$

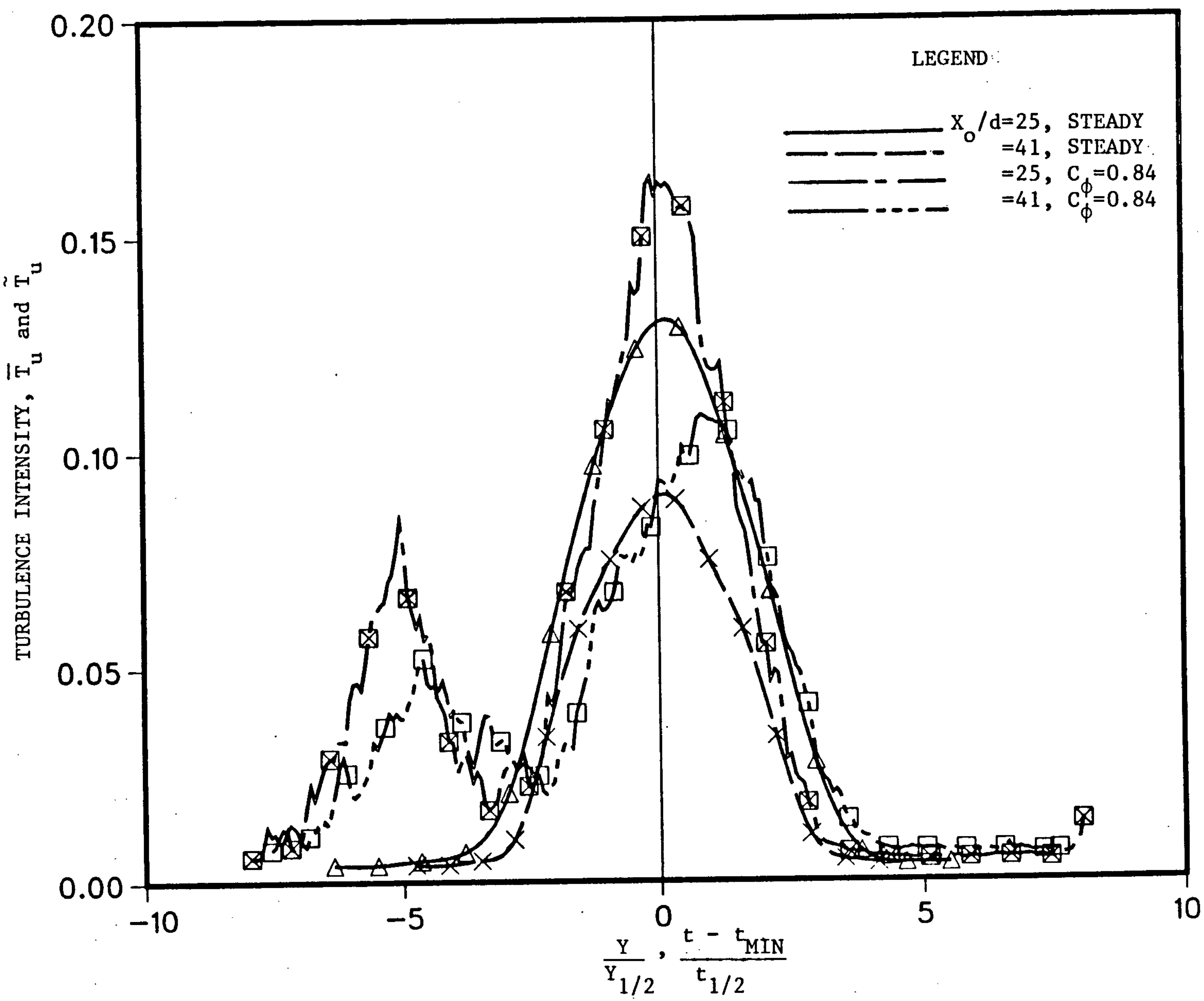

FIG. 4.8 NONDIMENSIONAL WAKE TURBULENCE INTENSITY PROFILES
$Re_d \simeq 5000$

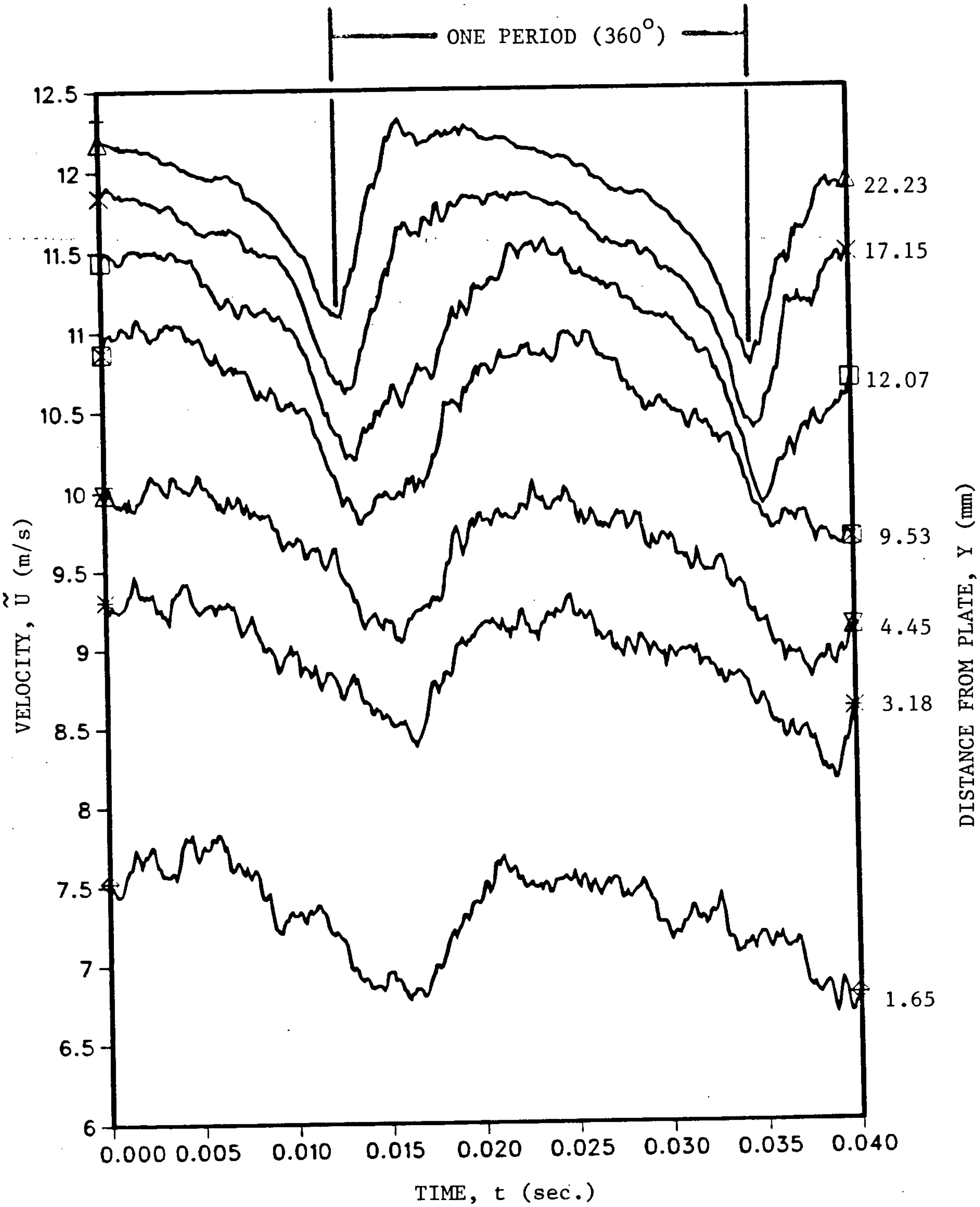

FIG. 4.9 ENSEMBLE-AVERAGED TIME-VELOCITY RECORDS AT $\overline{U}_\infty$= 11.75 m/s, ω= 50 Hz AND X= 200 mm

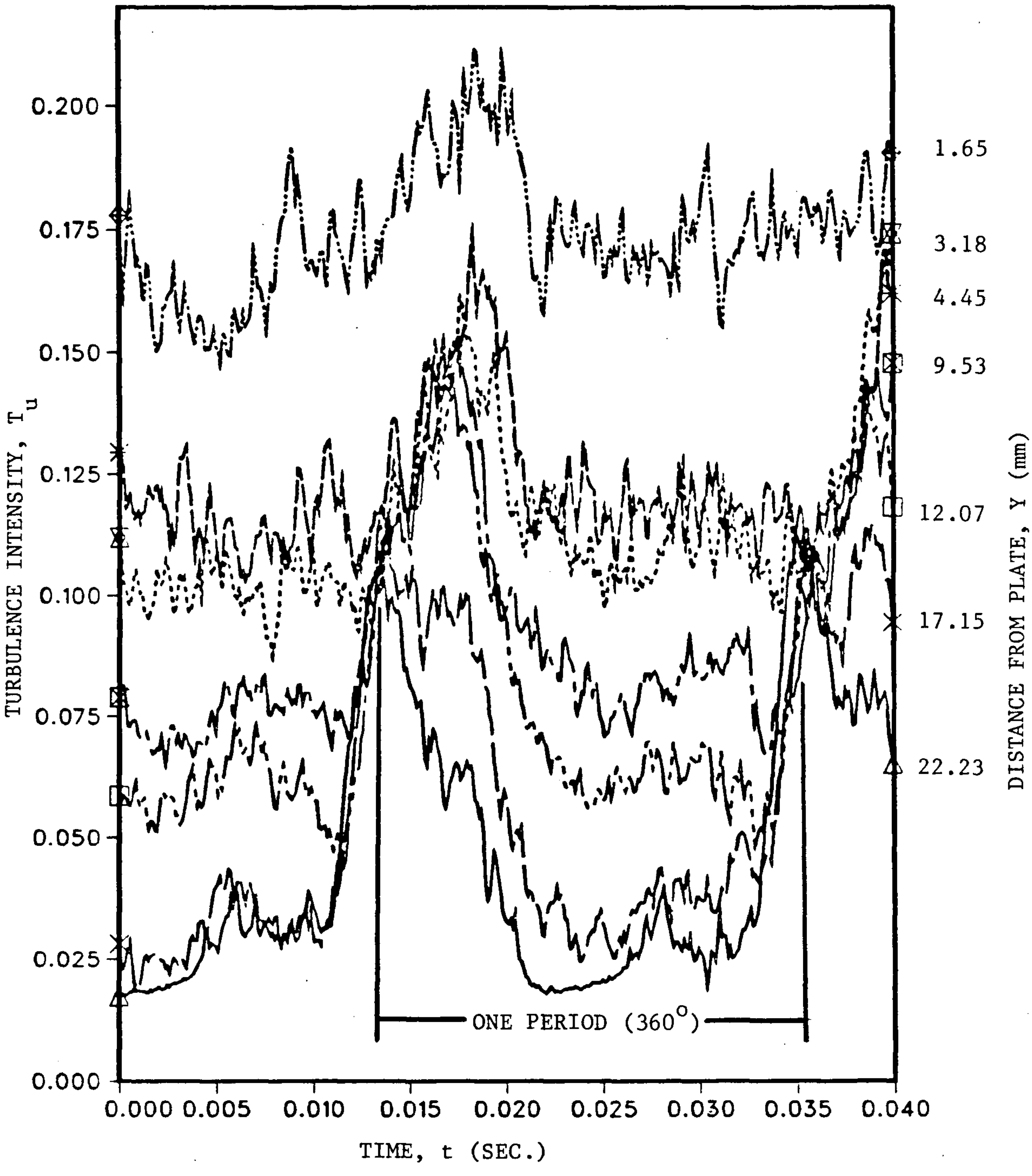

FIG. 4.10 ENSEMBLE-AVERAGED TURBULENCE INTENSITY-TIME RECORDS AT $\overline{U}_\infty$= 11.75 m/s, ω= 50 Hz AND X= 200 mm

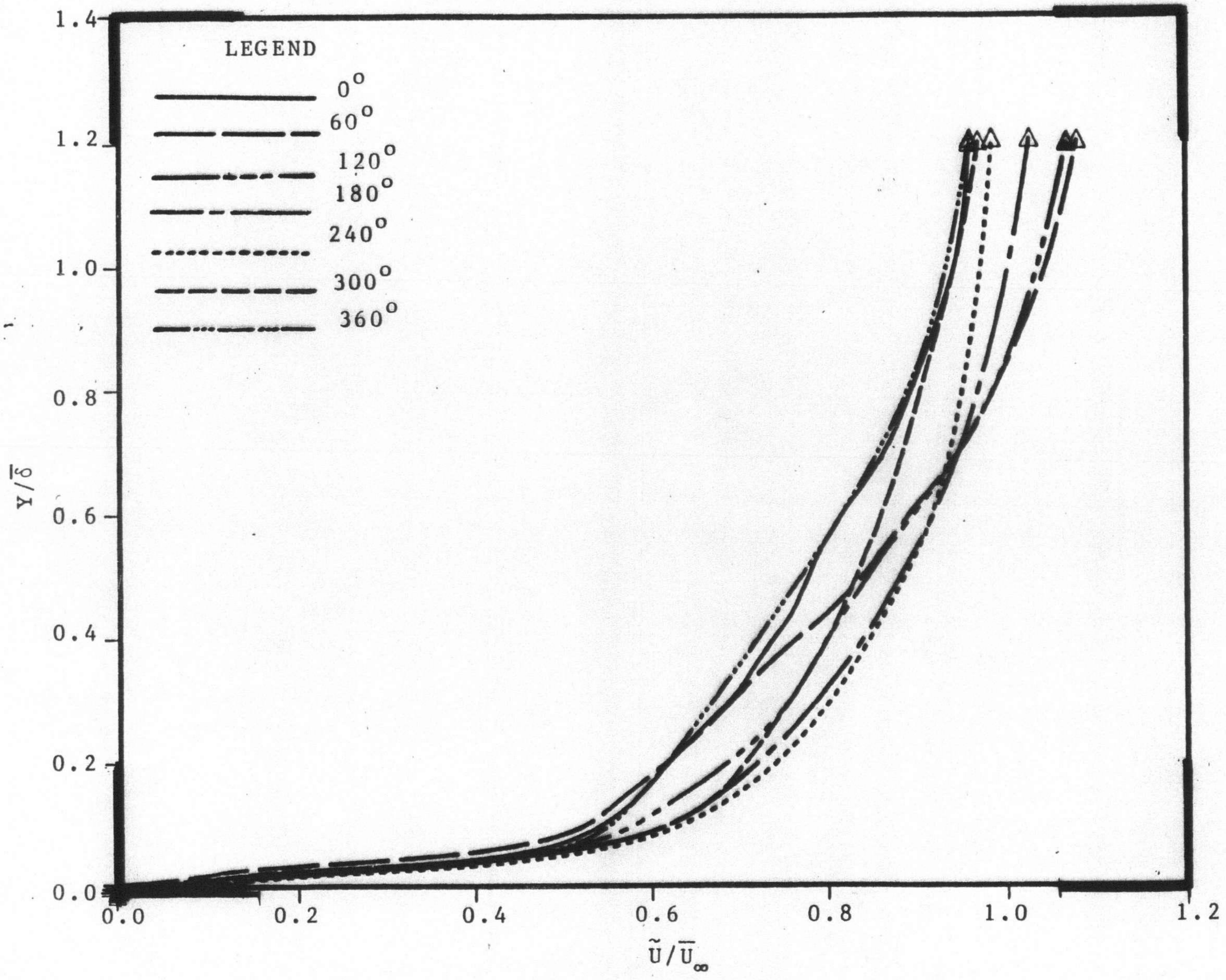

FIG. 4.11 NONDIMENSIONAL ENSEMBLE-AVERAGED VELOCITY PROFILES AT DIFFERENT PHASES, $C_\phi = 0.84$, $Re_x = 0.7 \times 10^5$

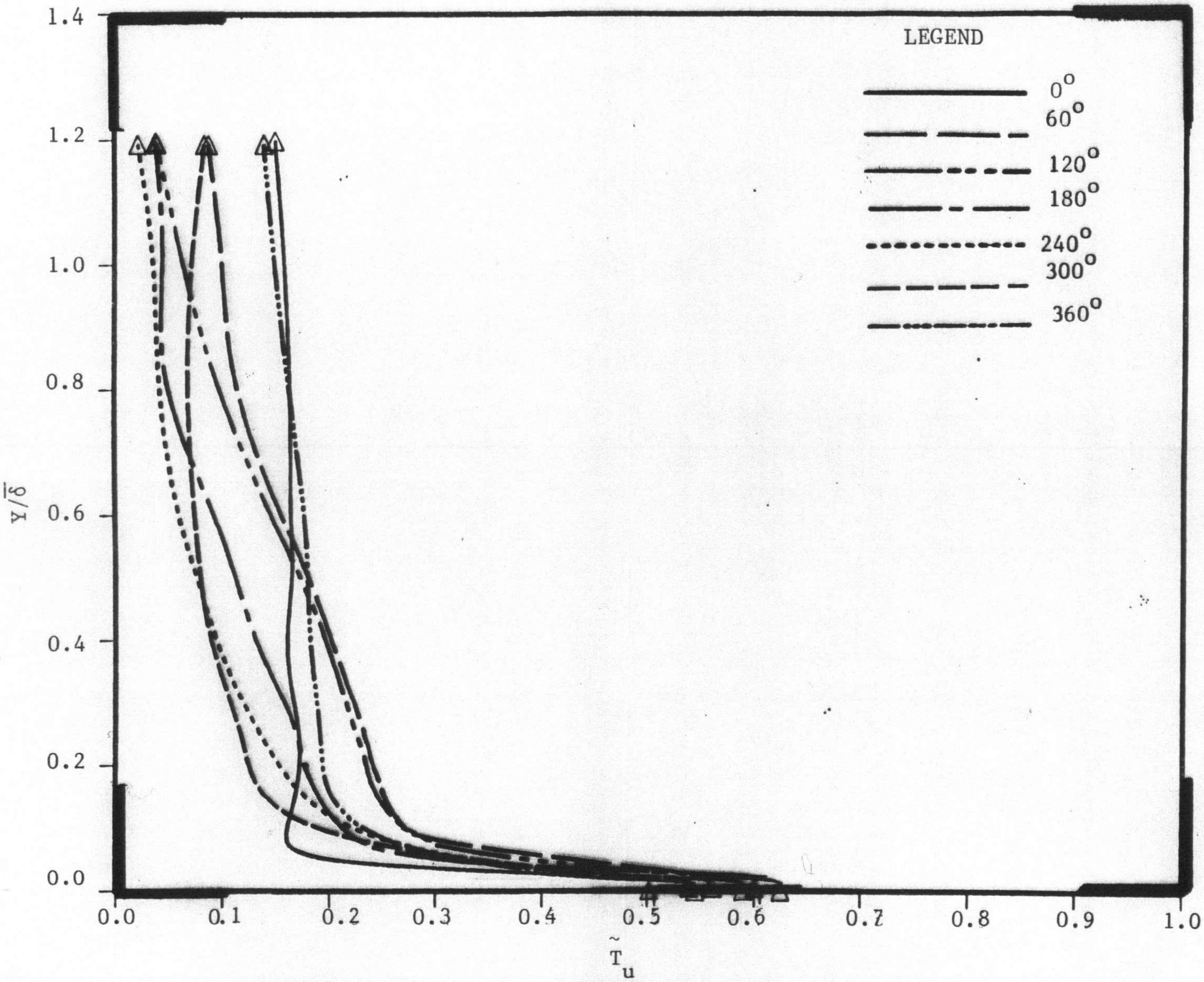

FIG. 4.12 NONDIMENSIONAL ENSEMBLE-AVERAGED TURBULENCE INTENSITY PROFILES AT DIFFERENT PHASES, $C_\phi = 0.84$, $Re_x = 0.7x10^5$

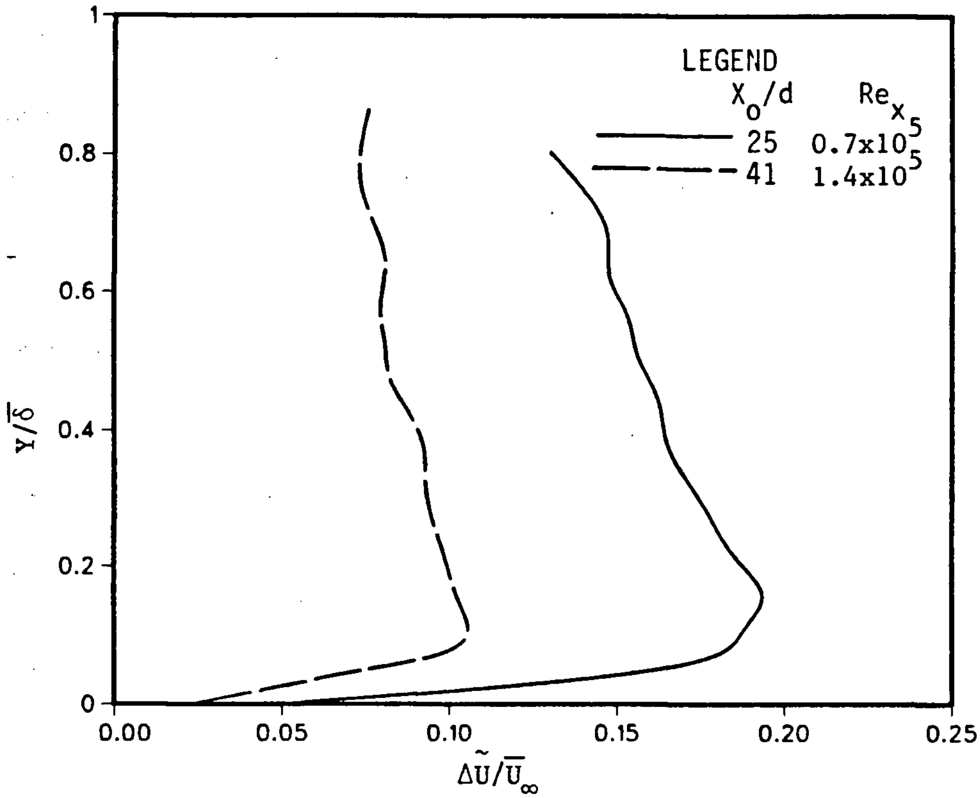

FIG. 4.13 MAXIMUM AMPLITUDE RATIO PROFILES, $C_\phi = 0.84$

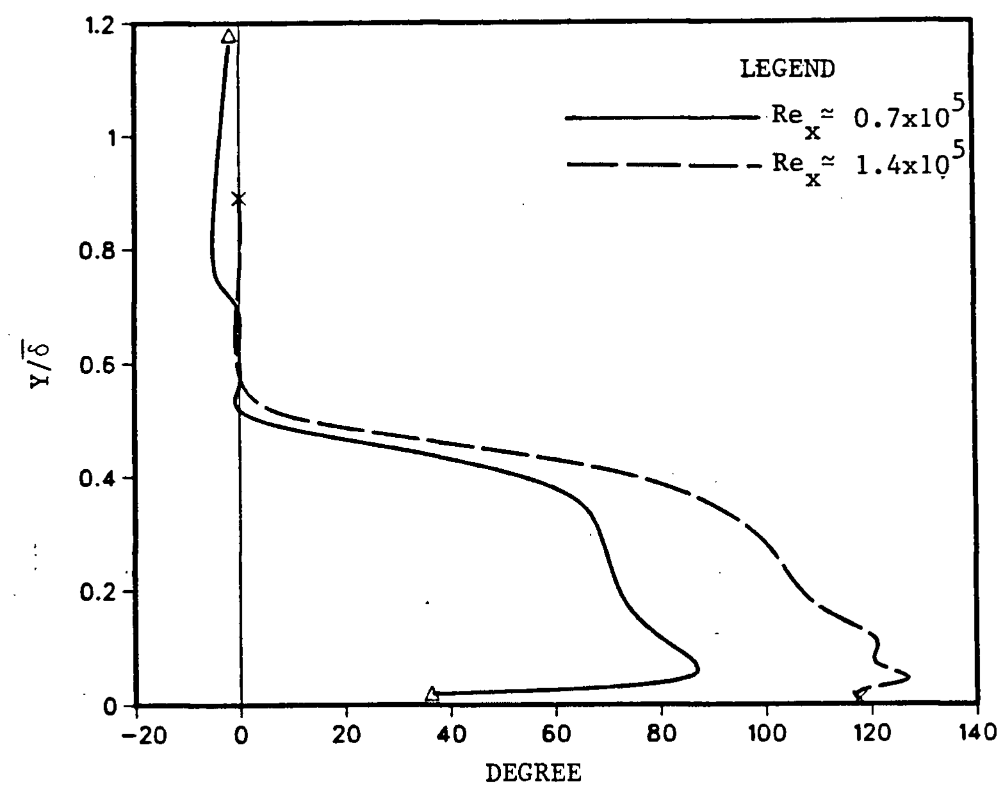

FIG. 4.14 PHASE LAG PROFILES, $C_\phi = 0.84$

REFERENCES

1. Binder, A., Forster, W., Kruse, H. and Rogge, H. (1984)
An experimental investigation into the effects of wakes on the unsteady turbine rotor flow.
A.S.M.E. paper 84-GT-178

2. Carr, L.W. (1981)
A review of unsteady turbulent boundary-layer experiments.
N.A.S.A. TM 81297

3. Cebeci, T. and Carr, L.W. (1978)
A computer program for calculating laminar and turbulent boundary layers for two-dimensional time-dependent flows.
N.A.S.A. TM 78470

4. Dixon, S.L. (1978)
Thermodynamics and fluid mechanics of turbomachinery.
3rd ed., Pergamon Press

5. Evans, R.L. (1973)
Turbulent boundary layers on axial-flow compressor blades.
Ph.D. dissertation, University of Cambridge.

6. Evans, R.L. and Horlock, J.H. (1974)
Calculation of the development of turbulent boundary layers with a turbulent free-stream.
A.S.M.E. paper 74-FE-24

7. Evans, R.L. (1977)
Boundary-layer development on an axial-flow compressor stator blade
A.S.M.E. paper 77-GT-11

8. Hodson, H.P. (1983)
Unsteady boundary layers on axial-flow turbine rotor blades.
Ph.D. dissertation, University of Cambridge.

9. Karlsson, S.K.F. (1958)
An unsteady turbulent boundary layer.

J.F.M., Vol. 5, pp.622-636

10. Langston, L.S. and Boyle, M.T. (1982)
A new surface-streamline flow-visualization technique.
J.F.M., Vol. 125, pp.53-57

11. Massey, B.S. (1968)
Mechanics of fluid.
2nd ed., Van Nostrand Reinhold co.

12. Marumo, E., Suzuki, K. and Sato, T. (1977)
A turbulent boundary layer disturbed by a cylinder.
J.F.M.,Vol. 87, part 1, pp.121-141

13. Patel, M.H. (1977)
On turbulent boundary layers in oscillatory flow.
Proc. Roy. Soc. (London) A353 pp.121-144

14. Pfeil, H., Herbst, R. and Schroder, T. (1982)
Investigation of the laminar-turbulent transition of boundary layers disturbed by wakes.
A.S.M.E. paper 82-GT-124

15. Schlichting, H. (1979)
Boundary layer theory.
7th ed., McGraw-Hill

16. Schlichting, H. and Das, A. (1967)
On the influence of turbulence level on the aerodynamic losses of axial turbomachines.
in, Flow research on blading
ed., L.S. Dzung, Elservier publishing co.

17. Tsiolakis, E.P. Krause, E. and Muller, U.R. (1983)
Turbulent boundary layer-wake interaction.
4th Sym. on turbulent shear flow, Sept. 12-14, 1983, Karlsruhe, F.R. Germany.

APPENDICES

APPENDIX A TURBULENCE INTENSITY FROM UNLINEARIZED CONSTANT TEMPERATURE ANEMOMETER (CTA) OUTPUT

The connection between the instantaneous velocity variation, u, and the AC component of the CTA output is

$$u = \frac{e}{dE_c/dU} \qquad \text{A.1}$$

and thus the root-mean-square relationship is,

$$\sqrt{\bar{u}^2} = \frac{\sqrt{\bar{e}^2}}{dE_c/dU} \qquad \text{A.2}$$

E_c is the ÇTA mean voltage and U is the mean flow velocity. dE_c/dU is, therefore, the slope of the calibration curve, $E_c = f(U)$, which is according to the calibration expression;

$$E_c{}^2 = A^2 + BU^n \qquad \text{A.3}$$

From A.3, the derivative of E_c with respect to U is

$$(dE_c/dU) = (nBU^{n-1})/2E_c \qquad \text{A.4}$$

As a result,

$$\sqrt{\bar{u}^2} = ((2E_c)/(nBU^{n-1}))\sqrt{\bar{e}^2} \qquad \text{A.5}$$

The turbulence intensity can be obtained from the unlinearized hot wire ouput according to the following equation.

$$\left(\sqrt{\bar{u}^2}/U \right) = \left((2E_c)/(nBU^n) \right) \sqrt{\bar{e}^2} \qquad \text{A.6}$$

APPENDIX B CALCULATIONS OF INTEGRAL BOUNDARY LAYER PARAMETERS: DISPLACEMENT THICKNESS AND MOMENTUM THICKNESS

The displacement thickness, δ^*, is the distance which the surface would have to be displaced outwards to reduce the total flow of a frictionless fluid by the same amount reduced by a real boundary layer. Similarly, the momentum thickness, θ, is the thickness through which the total reduction of fluid momentum under frictionless conditions is equal to that of a real boundary layer. They are calculated from the boundary layer data according to the following equations,

$$\delta^* = \int_0^\infty (1-(U/U_m))\ dy \qquad \text{B.1}$$

and,

$$\theta = \int_0^\infty (U/U_m)(1-(U/U_m))\ dy \qquad \text{B.2}$$

U and U_m are mean velocities in the boundary layer and free stream. The integrations of the experimental data are carried out by a UBC computer library integration routine, QINT4P, which is for integration of unequally spaced data points using the quadrature method.

APPENDIX C ESTIMATION OF BOUNDARY SURFACE SHEAR STRESS COEFFICIENTS BY CLAUSER PLOTS

This technique is to estimate the surface shear stress coefficient, C_f, from the shape of a velocity profile. However, the shape of the velocity profile has to agree with the shape of the "Law of the Wall" profile, section 2.1, in order to use this technique.

$$\frac{U}{u_\tau} = \frac{1}{K} \ln\left(\frac{y u_\tau}{\nu}\right) + C \tag{C.1}$$

where $u_\tau = (\tau_w/\rho)^{1/2}$ C.2

and $C_f = (\tau_w/(\frac{1}{2}\rho U_\infty{}^2))$ C.3

from C.3,

$$\frac{\tau_w}{\rho} = \frac{1}{2} U_\infty{}^2 C_f \tag{C.4}$$

substitute C.4 into C.2 and then into C.1,

$$\frac{U}{U_\infty (C_f/2)^{1/2}} = \frac{1}{K} \ln((y U_\infty (C_f/2)^{1/2})/\nu) + C \tag{C.5}$$

from C.5,

$$\frac{U}{U_\infty} = \left(\frac{C_f}{2}\right)^{1/2} \frac{1}{K} \ln\left(\frac{y U_\infty}{\nu}\right) + \left(\frac{C_f}{2}\right)^{1/2} \left(C + \frac{1}{K} \ln\left(\frac{C_f}{2}\right)^{1/2}\right) \tag{C.6}$$

which can be simplified to

$$\frac{U}{U_\infty} = m(\ln \frac{yU_\infty}{\nu}) + b \qquad C.7$$

where $m = (C_f/2)^{1/2}/K$

$$b = (C_f/2)^{1/2}(C + \ln(C_f/2)^{1/2}/K)$$

By substituting different C_f values into equation C.7, the linear relationship between U/U_m and $\ln(yU_\infty/\nu)$ can be plotted as shown in Fig.C.1. A velocity profile which agrees with the "Law of the Wall" should have a linear region which is parallel to the straight lines when it is plotted according to equation C.7. As a result, the surface shear stress coefficients can be estimated.

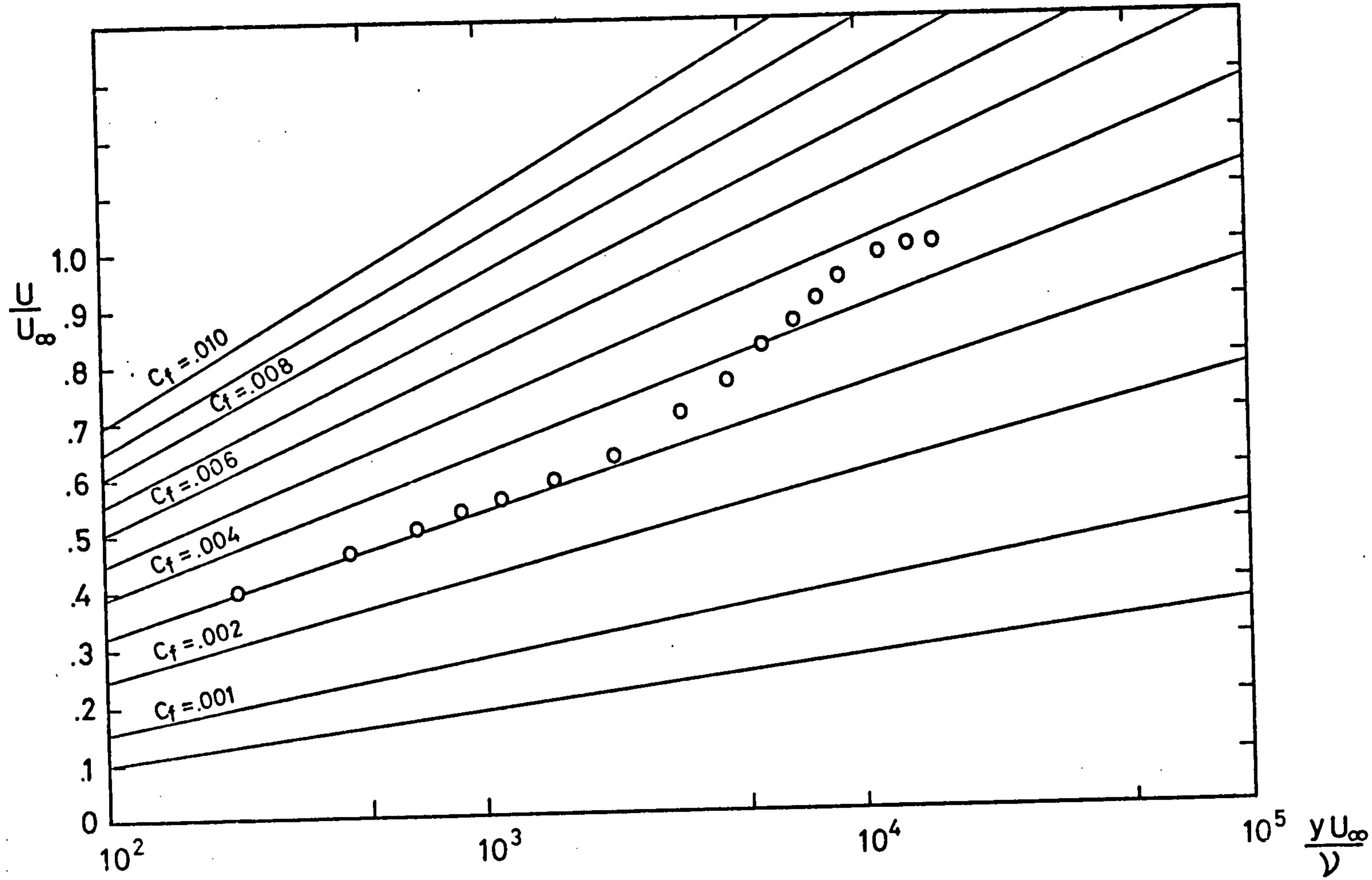

FIG.C.1 TYPICAL CLAUSER PLOT (EVANS 1973)